Detection and Segmentation of Stroke Lesions from Diffusion Weighted MRI Data of the Brain

Thesis submitted in partial fulfillment
of the requirements for the degree of

MS by Research
in
Computer Science

by

Shashank Mujumdar
200702042
shashank.mujumdar@research.iiit.ac.in

Centre for Visual Information Technology
International Institute of Information Technology
Hyderabad - 500 032, INDIA
July 2013

International Institute of Information Technology
Hyderabad, India

CERTIFICATE

It is certified that the work contained in this thesis, titled "Detection and Segmentation of Stroke Lesions from Diffusion Weighted MRI Data of the Brain" by Shashank Mujumdar, has been carried out under my supervision and is not submitted elsewhere for a degree.

Date	Advisor: Prof. Jayanthi Sivaswamy

To My Parents

Acknowledgments

First and foremost, I would like to express my sincere gratitude to my advisor Prof. Jayanthi Sivaswamy for showing me the path to being a true researcher. With her immense knowledge and experience, her keen interest in my research and her able guidance, I was able to deliver this thesis. I can only thank her for her patience, motivation, enthusiasm, constant support and shaping my attitude towards research. I was really fortunate to have her as my guide on this remarkable journey.

I share the credit of my work with Dr. Dattesh Shanbhag and Dr. Rakesh Mullick from GE Global Research, Bangalore, India. They gave me key insights into the work, constructive criticism and valuable inputs that benefited my work. I would also like to thank Dr. L.T. Kishore and Dr. Ravi Varma from CARE Hospital, Hyderabad, India for providing me with the knowledge of medical practices, medical data and the ground truth required for my work. Their invaluable contribution helped me understand the clinical significance of my work and helped me design the proposed framework.

I was fortunate to have Gopal, Sai and Harini as my mentors at CVIT. They have been an inspiration and have influenced both my personal and professional life. I thank them for their constant guidance and support and motivating me in times of despair. I am thankful to my peers at CVIT and my friends who have always been there, making the journey fun and a memorable one - Saurabh, Karthik, Sandeep, Ujjwal, Rohit, Akhilesh, Parikshit, Nigam, Sahni, Chandra, Sureka, Abhinav, Vinay, Baronia, Siddhartha, Ankur, Yasir, Sankalp, Pawan, Rakshit, Romit, Shubhangi, Sruti and others.

Finally, I am grateful to my parents for being the pillars of support and believing in me. With their presence I always felt content and I am indebted for life to them.

Abstract

Stroke is a chronic disease which often leads to death. Different medical imaging modalities enable diagnosis for stroke after the onset of symptoms. Time is of the essence during stroke analysis since the window of therapy is very small ($<$ 3 hrs after the onset of symptoms). Recent clinical studies have shown the usefulness and significance of diagnosing stroke on the *Diffusion Weighted Magnetic Resonance Imaging* (DWI) scans of the brain in the early stages. Visual inspection of the DWI scans is difficult since multiple scans are acquired for a patient with varied contrast and the scans depict complementary information about the diffusion process in the brain. To make matters worse, the DWI scans are acquired at a very low resolution with poor signal to noise ratio (SNR) since the time of acquisition is significantly less ($<$ 1 min) and are confounded by artifacts that mimic stroke lesions. Thus, an automated framework which can accurately capture the stroke lesions in the DWI data would assist the clinicians in a better diagnosis. This is focus of the thesis.

Varying the acquisition parameter (*b-value*) generates different DWI scans with varied contrast. DWI with higher b-values provide improved sensitivity, conspicuity of stroke lesions and reduced artifacts at the cost of lower SNR. Along with the DWI scans, the Apparent Diffusion Coefficients (ADC) maps are also derived which give a measure of the true diffusion process in the brain irrespective of the acquisition artifacts that resemble stroke. In this thesis, we argue that integrating information from multiple sources, namely, low and high b-value data along with the ADC maps, can aid better characterization of stroke lesions in the data. Accordingly, we propose a novel approach for detecting and segmenting stroke regions from DWI data.

An automated framework comprising of 3 stages is proposed for accurately capturing the stroke lesions: (i) Stroke Detection (ii) Contrast Enhancement and (iii) Stroke Segmentation, utilizing information from low and high b-valued DWI data and the ADC maps. The detection stage utilizes the information from lower b-value data and the ADC data to identify the stroke lesions on the higher b-value data and reject the false positives due to low SNR in high b-value data. The detected stroke lesions are segmented using the higher b-value data and ADC information. Integrating information from the higher b-value data along with the ADC data helps better define the stroke lesion in the segmentation stage. An auto-windowing technique is designed to enhance the contrast of the stroke lesions in the DWI data prior to segmentation. The contrast enhancement scheme also assists the radiologists in the manual/visual diagnosis of stroke in DWI scans.

The proposed method was evaluated on datasets acquired from different scanners with different acquisition protocols. The performance evaluation of the proposed approach validates its robustness and effectiveness. Receiver operator characteristic (ROC) analysis shows high values of sensitivity, specificity and area under the curve. The proposed system achieves a sensitivity of 0.96 at a specificity of 0.95 with the area under the receiver operating characteristic curve (AUC) of 0.987. Qualitative and quantitative analysis of the results presented in the study establish the strength and robustness of the method in capturing the small-sized lesions in the data which are often missed by segmentation methods operating on a single b-value data.

Contents

List of Figures

List of Tables

Chapter 1

Introduction

1.1 Foreward

"It was an usual day, a few weeks after my fifteenth birthday. That day, I remember that I had soreness down the left side of my body, along with what I thought was a bad headache. I didn't feel quite right, but I thought that this was nothing to get concerned about. Neither did my parents. The headache, along with other symptoms, which I now realize were warning signs of stroke, were things I had experienced before. Then the pains had disappeared after a few hours. I put these down to crankiness, eye-strain, or teenage growing pains. That night, I went off to bed, thinking that I would feel fine in the morning. The next thing I remember was waking up in the intensive care ward at the local hospital. I was eventually moved out of intensive care into a ward. I was paralysed down the left side of my body, and had a bandage around my head. Then came the day when the doctors explained what had happened to me. I was told that I had suffered a massive stroke." - A stroke survivor shares his experience of the tragic incidence and how the person fought against it with the support and encouragement from his family and friends to make the recovery [2]. This is a typical story of every stroke survivor of his/her experience of its dreadful incidence. Stroke is one of the deadliest medical conditions that can occur to an individual. However, with the technological advances and years of research it is now possible to address this condition of an individual and change the course of fate. Such an idea for a potential technological development for treatment of stroke is presented in this dissertation. Let's first get ourselves acquainted with *stroke* and its effects.

1.2 Stroke

1.2.1 What is Stroke?

Stroke is a medical condition caused due to inadequate supply of blood (lack of oxygen and nutrients) to the brain cells which damages them and may result in their death. Blood flow may be interrupted due to one of the following:

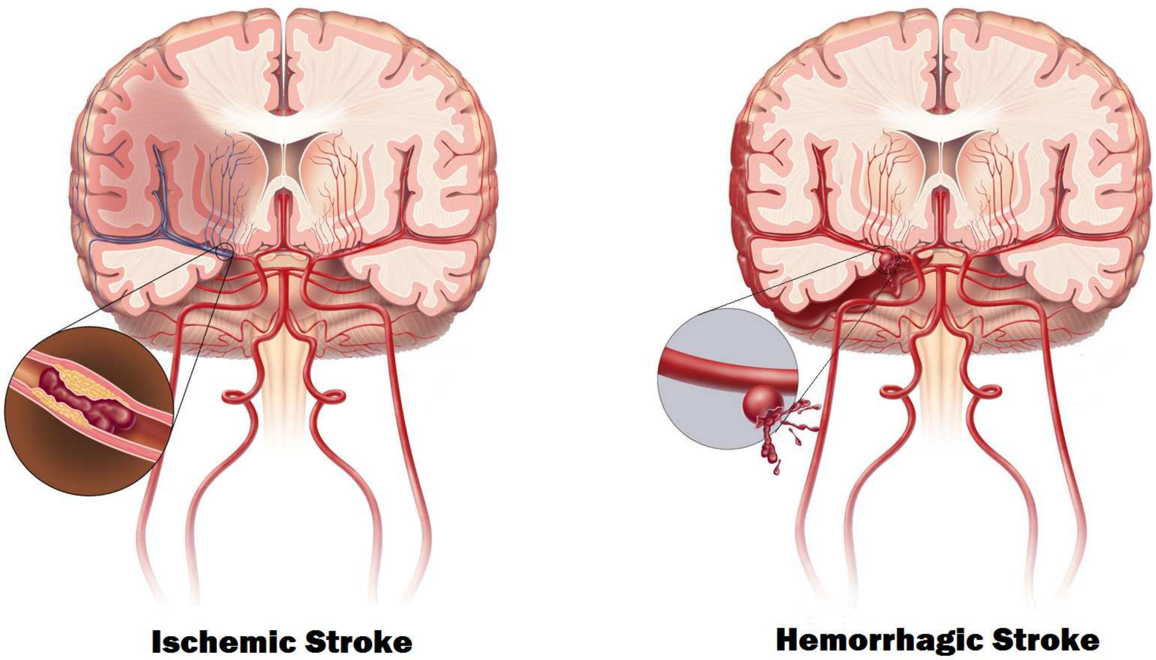

Figure 1.1: Ischemic and Hemorrhagic strokes and corresponding affected regions in the brain (image courtesy [1]). The zoomed sub-image shows a vessel clot in the case of ischemic stroke. In the case of hemorrhagic stroke the zoomed sub-image shows a vessel rupture.

- A clot in the blood vessel occludes the supply.
- A blood vessel rupture disturbs the supply.

Stroke caused due to a clot in the blood vessel is referred to as *ischemic* stroke and that due to a blood vessel rupture is referred to as *hemorrhagic* stroke. Figure 1.1 shows these two types of strokes in the brain. In the ischemic stroke, the region deprived of the blood supply (due to a clot) is shown while in case of hemorrhagic stroke the blood starts to spill inside the brain regions (due to vessel rupture). Interruption in the blood supply disrupts the supply of oxygen and essential nutrients to the brain cells and hence damages them. The inadequacy or the loss of oxygen and nutrients to the brain cells is referred to as *ischemia* which ultimately leads to their death termed as *infarction* or *ischemic* stroke. Ischemic stroke accounts for around 80% of all strokes. Stroke is the third most common cause of death, after cancer and ischemic heart disease. Its incidence is accelerating in developing countries due to unhealthy lifestyles. A stroke kills around 32,000 brain cells in a second. $1/5^{th}$ of the victims die within a month of its occurrence and half of the survivors become physically disabled.

1.2.2 Effects of Stroke

Stroke adversely affects a person's life forcing a change in their life-style and possibly lead them to reconstruct their identity. The occurrence of a stroke is sudden and incapacitating. Even for stroke cases

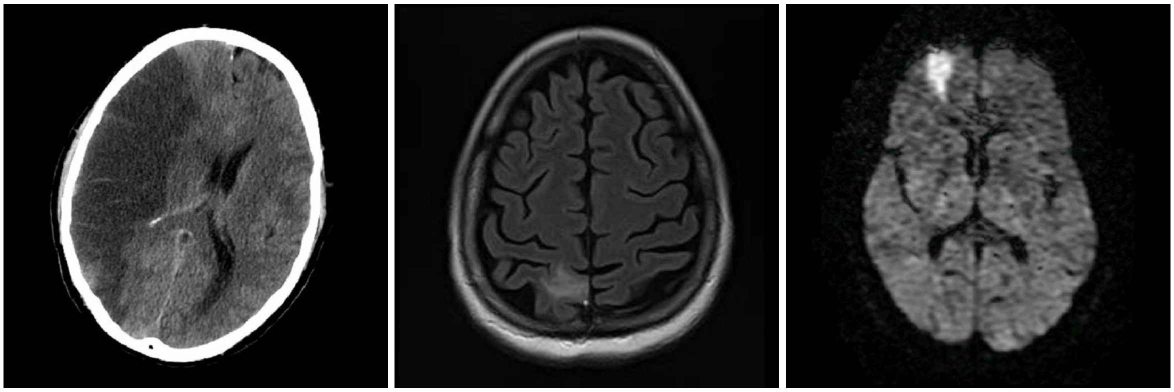

Figure 1.2: Ischemic Stroke as seen on (a) CT scan - seen as a slightly dark region (b) MRI scan - seen as a slightly bright region (c) DWI scan - seen as a distinctively bright region.

of minor severity, the recovery is often a long-term process. The future of a stroke survivor involves a series of physical, psychological, behavioural and social challenges. There is often the uncertainty of the recurrence of the stroke. Weakness, numbness or complete paralysis observed in one side of the body, is a common disability among stroke survivors. Weakness in the muscles used for breathing, producing voice and speech is seen among the survivors which results in slurred speech and heavy breathing while talking. The cognitive abilities of a survivor such as thinking, awareness, self-confidence might be affected. These factors affect the independence of the individual and require to be worked upon in order for the survivor to again be socially active. Loss of memory, loss of control over emotions and feelings of frustration are also common features observed among the survivors. A stroke can be devastating, which is why it's important to minimize the risk with prompt treatment.

1.2.3 Treatment and Therapy

Hippocrates, the father of western medicine [14], identified stroke as a sudden onset of paralysis. In ancient times, little was known among the physicians for its cause and no standard therapy was established. However, modern medicine provides several techniques for stroke diagnosis. Evaluating the patient on a neurological examination [26] (NIHSS), in-vivo imaging techniques such as Computed Tomography (CT), Magnetic Resonance Imaging (MRI), Diffusion Weighted Imaging (DWI) for diagnosis and thrombolytic therapy with tissue plasminogen activator (tPA) within 3 hours of ischemic stroke [13] onset are the established practices followed for stroke diagnosis and treatment.

The core of the region to which the blood supply is interrupted shows significant cell death in the brain tissue while some cells surrounding the core (penumbra) are damaged and can be saved with timely treatment. Early and accurate evaluation of presence of infarct (core) and its extent (prenumbra) is most important in the setting of acute stroke since it helps the clinicians to classify the stroke sub-type and plan for treatment. The primary task is to diagnose the acute stroke and identify the core and classify the tissue at risk which is salvageable. The DWI data help identify the core of the ischemic stroke lesion as a bright region in the scan. On the other hand, perfusion weighted magnetic resonance imaging (PWI) provides information on the impaired perfusion (blood flow through vessels of the brain) in the core and surrounding brain regions. The PWI represents a quantitative data and hence the region of interest (penumbra of the stroke region) can be obtained easily. Extracting the region of interest on the DWI (core of the stroke region) requires manual delineation of the boundary of the stroke region by expert radiologists. Such a task depends on the availability of experienced radiologists and is time consuming. Hence, an automated framework which can accurately detect and segment the stroke lesions will aid the radiologist in a faster and accurate diagnosis.

MRI and CT are increasingly used by clinicians for diagnosis of neurological disorders. Identification of major ischemic change in CT is popular because of the low cost and high speed of acquisition. However, MR based diffusion and perfusion analysis of the ischemic stroke is more sensitive for early stroke region identification as compared to CT, especially in the early stages [5]. Figure 1.2 shows sample images of ischemic stroke as seen on different modalities. The stroke is clearly visible in the DWI scan as opposed to a CT scan. DWI enables early identification of the stroke in the brain. In addition to early detection, measurement of the stroke volume is needed in therapy planning and assessment which is also possible with DWI. Different semi-automated and automated techniques have been proposed in literature to identify and segment the ischemic stroke lesions utilizing different medical modalities. A few approaches have tried to utilize the information from multiple sources to better quantify the stroke region.

1.3 Thesis Focus

Stroke lesions appear hyper-intense on DWI and are inhomogeneous, with complex shapes and ambiguous boundaries with observed intensity variation [23] which makes manual segmentation difficult and time consuming. Multi-modal approaches presented in literature have aimed at tissue classification and identifying the salvageable regions during the evolution of stroke which assists the clinicians in predicting the eventual outcome in the chronic stage of the stroke. However, *early* detection and segmentation of regions of ischemic stroke, regardless of size and location, is critical for treatment. The conventional methods for stroke segmentation fail to capture the smallest regions of infarction in the scan.

The focus of this thesis is to accurately and automatically detect and segment the ischemic stroke lesions by utilizing the DWI data. The main challenge is detecting and segmenting the small-sized stroke lesions in the data. The problem of detection is twofold - (i) automatically localising the stroke lesions in the data (ii) enhancing the data for manual/visual analysis by experts. The challenge in task (i) is to accurately detect all the lesions regardless of their size. In order to accurately segment the stroke lesions in the data a pre-processing stage is required to enhance the conspicuity and the definition of the stroke lesions in the data. At the same time, standardizing display conditions for DWI scans on a standard 8-bit display has not been achieved. Thus, the challenge in task (ii) is to propose a contrast enhancement scheme that better defines the stroke lesions in the data and aids the segmentation process as well as provides standard displaying conditions for the radiologists to better diagnose the DWI scans for stroke lesions. As described earlier, the appearance of the stroke lesions in the DWI data is not well defined. Thus, the next challenge is to propose a method robust to the shape complexity and intensity inhomogeneity of the stroke lesions in the data in order to accurately segment them.

We investigate the idea of utilizing information from multiple b-value data and the ADC maps and propose a novel framework for combining information from b1000, b2000 DWI scans for stroke detection and segmentation. Details of how the scans are acquired and what they represent are mentioned in further chapters.

1.4 Thesis Contributions

The thesis presents a novel framework for processing (detection and segmentation) of ischemic stroke in a DWI scan. The major contributions of the thesis are:

- **Auto-windowing Technique:** We present a novel auto-windowing technique for enhancing the DWI scan relative to the ischemic stroke lesions. The work is motivated by both technical and clinical applications. Technically, it is used as a pre-processing stage for improving the contrast and the boundary definition of the ischemic stroke lesions in the data and hence improving the detectability and the segmentation results for image processing algorithms. Clinically, radiologists routinely use the windowing approach by manually varying the window parameters to better diagnose the region of interest. However, this task is cumbersome and there is no standardization. To date there is no literature available on automating the windowing task and providing a standard for this windowing approach. We provide an efficient algorithm to automate the windowing process and in order to validate the clinical significance of the approach a perception study with expert radiologists is carried out and extensive analysis of the obtained results is done.

- **Detection of Ischemic Stroke Integrating Information from Multiple b-Value DWI and the ADC Maps:** We propose a novel method for accurately detecting ischemic stroke lesions from DWI data. The detection of the candidate lesions and the task of addressing the false positives is achieved by unifying supplementary information from multiple b-valued data and the ADC maps. Analysis of the detection results shows our method is able to accurately detect the smallest regions of infarction in the data.

- **Accurate Segmentation of Ischemic Stroke Lesions:** An extension of the Chan-Vese [9] formulation for active contours is proposed for segmentation of stroke lesions. The extension operates on a vector image, as opposed to a scalar image in the standard formulation, exploiting information from multiple image sources to better define the contour evolution.

- **Implementation of Automated Pipeline:** An automated algorithm employing the proposed framework is implemented in MATLAB [28].

1.5 Thesis Organization

The organization of the thesis is as follows. Chapter 2 discusses about the medical imaging modalities for processing stroke. The concept of DWI is introduced and the acquisition process of DWI with multiple b-values is explained. This chapter lays the foundation for the significance of DWI and the measures to be taken in processing ischemic stroke. The proposed multi-stage pipeline is introduced in the chapter. The corresponding sub-stages of the pipeline are discussed in brief and the need for introduction of the respective sub-stages is justified. The novelty of the proposed system utilizing information from multiple b-values is discussed in brief.

The DWI data is inherently noisy with low resolution and hence a novel auto-windowing technique is proposed in Chapter 3 as a preprocessing stage before the actual segmentation task is performed. The goal is to find the window setting that maximizes the local contrast for the lesions in a given dataset. For every given candidate, the local contrast is measured for a set of window parameters. The desired *best* window is the one which yields maximum local contrast for the lesions. A detailed analysis of the windowing results is presented. Results of a perception study of the windowed results against 8 radiologists are also presented to validate the results of the approach from a clinical point of view.

Chapter 4 discusses the proposed system for detection and segmentation of ischemic stroke lesions in the DWI scans in detail. The method utilizes information from multiple b-values to accurately detect the lesions in the data. An extended version of the Chan-Vese [9] formulation of active contours is proposed for final segmentation using the candidate lesions as the input. A detailed analysis of the segmentation results to validate the proposed system is presented. Performance evaluation of the approach against a leading method [8] as well as against the proposed system utilizing single b-value data is also presented.

Chapter 5 concludes the work and discusses the potential application of the proposed system in clinical usage and the challenges to be faced to envision this goal.

Chapter 2

Background Work and Proposed System

2.1 Medical Imaging Modalities for Stroke Diagnosis

CT is extensively used for identification of suspected stroke in the initial stages. Subtle changes in scan may reflect regions of cytotoxic edema which results in ischemia. The changes are generally reflected in the contrast at the junction that separates the tissue of gray matter and white matter in the scan. Early identification of ischemic changes in non-contrast CT is a challenge and depends on the reviewer experience. In the first 6 hours from the onset of the stroke, the CT scan fails to capture the early ischemic changes in most cases. Thus, in an emergency setting, CT is primarily used to rule out any intracerebral haemorrhage [5]. Use of CT angiography and CT perfusion aids the analysis of stroke on a CT scan, however, at the cost of additional contrast material and radiation exposure [17].

Conventional MRI is more sensitive to ischemic changes as compared to CT. Hydrogen nuclei (protons) in the human body become excited when positioned in a strong magnetic field; they absorb the radio frequency energy of the magnetic field and then release it until they relax completely. The energy is released from the excited tissue over a short period according to two relaxation constants known as T1 and T2, and the emitted energy signals are converted into images. The contrasts in the images result from different intensities of these emitted signals, which in turn result from different concentrations of the nuclei in different tissues in the body [19]. A subtle change in the contrast is easier to identify on the MRI. However, such changes are not usually visible upto 3-4 hours from the onset of stroke [4]. A few of the limitations of MRI are its high cost and long scanning durations making it difficult to exploit its use in emergency setting.

Diffusion-weighted imaging (DWI) is sensitive to the microscopic random motion of the water molecule protons. To obtain diffusion-weighted images, a pair of strong gradient pulses are added to the pulse sequence used in traditional MRI. The signal strength depends on the magnitude of molecular translation and diffusion weighting. The amount of diffusion weighting is determined by the strength of the diffusion gradients, the duration of the gradients, and the time between the gradient pulses. In areas of acute stroke the diffusion process is hindered and it is revealed as a hyper-intense signal in the acquired scan which forms the underlying phenomenon of stroke detection methods [12]. Clinical studies have proved that diffusion-weighted magnetic resonance imaging (DW-MRI) is more sensitive to early ischemic stroke than conventional MRI or CT and thus helps in the diagnosis of acute ischemic stroke at a stage when the lesions might not be detectable in other modalities [11].

2.2 Characteristics of Diffusion Weighted MRI

DWI encodes the mobility of the water molecules in the brain in to a sequence of images with varied contrast [15]. The signal intensity of the DWI scan at every voxel depends on the degree of diffusion of the water molecules in the underlying tissue. The diffusion process is hindered in locations of acute stroke and this manifests as a hyper-intense signal in the acquired scan [16][34]. The diffusion sensitivity during acquisition is quantified by the *b-value* which determines the strength and duration of the diffusion gradients. The b-value is a control parameter which is fixed for every scan. The b-value is calculated as

$$b = \gamma^2 G^2 \delta^2 (\Delta - \delta/3)$$

where, γ is the gyromagnetic ratio, G is the amplitude of diffusion gradients, δ is the duration of the diffusion gradients and Δ is the time interval between the two gradients. Increase in diffusion sensitivity (b-value) is usually accounted for by the increase in values of G and sometimes due to increase in values of δ and Δ.

Varying the b-value generates sequences with varied contrast for the same tissue [35]. The scan obtained with $b = 0$ is a standard T2 image, generally used as an anatomical reference. Increase in b-value serves to attenuate the signal intensity for the normal tissue more as compared to that of the lesion thus helping improve the contrast of the lesion. Accordingly, imaging with higher b-value in a 1.5 Tesla scanner has been found to improve the conspicuity, particularly for small-sized lesions and reduce the number of shine-through artifacts, however, at the cost of SNR degradation and accentuated anisotropic effects in regions where white matter tracts are prominent [10][23]. The signal strength depends on the echo time (TE) during acquisition. An increase in b-value results in an increase in TE and thus the SNR of the resulting scan is compromised. Figure 2.1 shows a slice obtained with multiple b-values: $b = 0$, $b = 1000$ and $b = 2000$. As seen from Figure 2.1, the stroke lesion has improved conspicuity and contrast in the $b2000$ scan relative to the $b1000$ scan. However, the $b2000$ scan appears noisier than the $b1000$ scan.

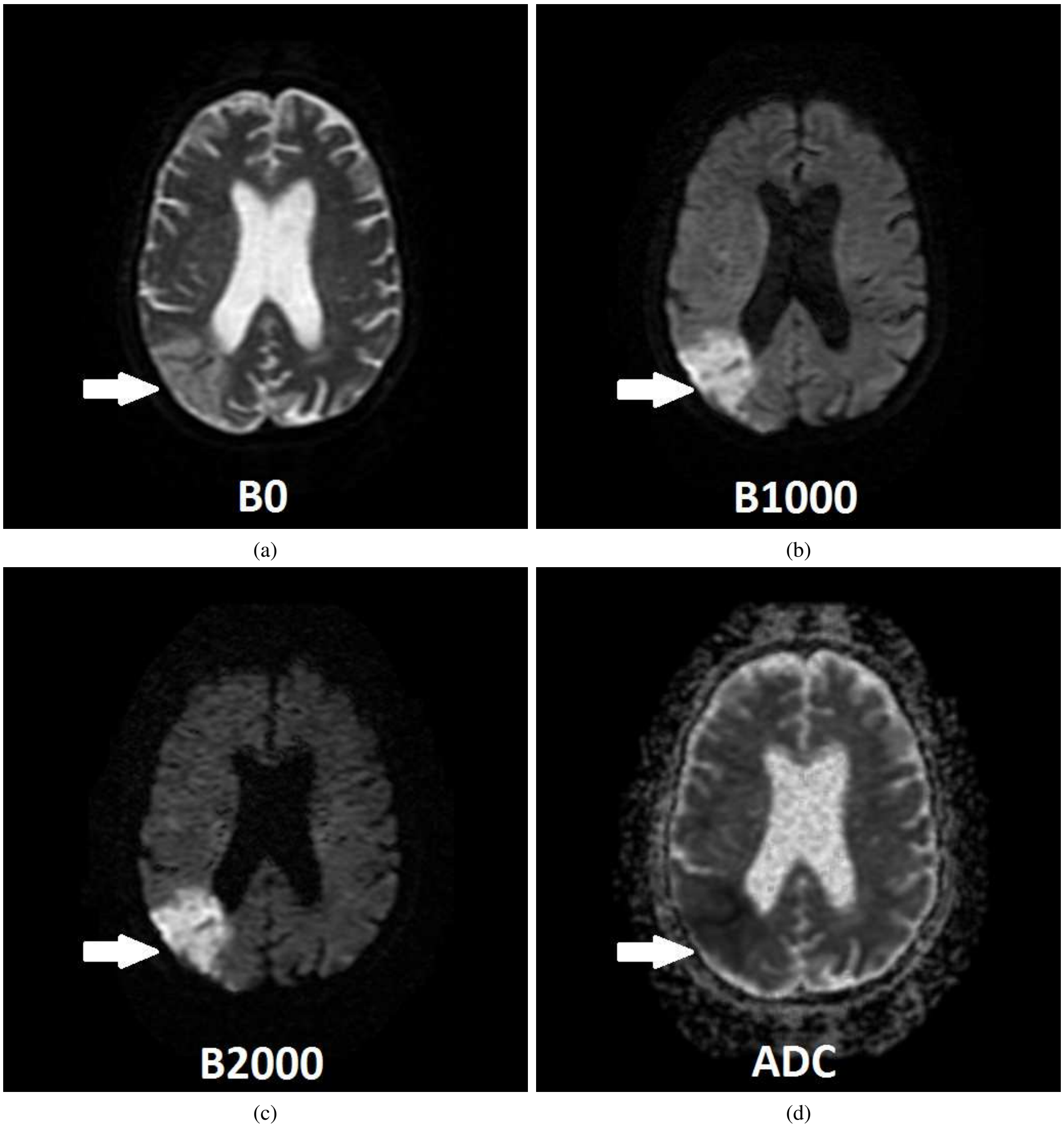

Figure 2.1: DWI scans with different b-values (a) b=0 (b) b=1000 (c) b=2000 and the corresponding ADC map. The arrow shows the region of stroke as seen on these different scans.

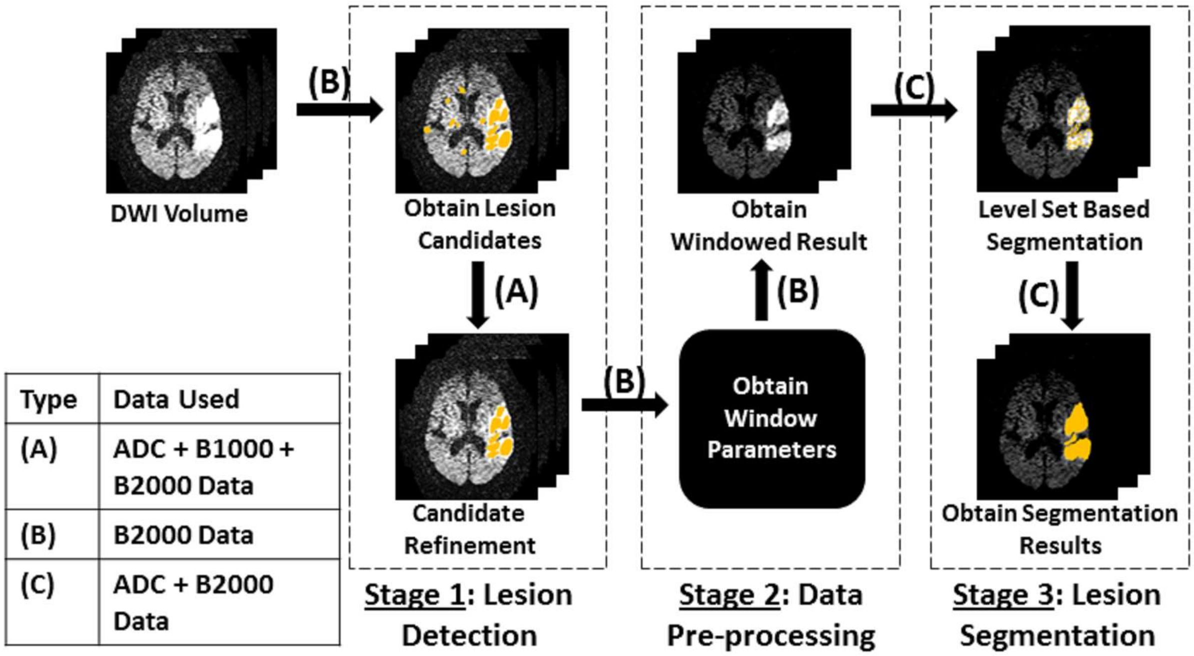

Figure 2.2: Processing pipeline of the proposed approach. The data used at every sub-stage is described in the legend.

Imaging with high b-value reduces the relative contribution of the T1 and T2 weighting in the acquired scan [10]. The signal intensity in DWI decays exponentially with the rate of diffusion in a voxel. The signal intensity in a DWI scan is confounded by the overlaying T2 signal intensity. Regions sensitized due to long T2 may simulate contrast similar to reduced diffusion [31]. Such artifacts are referred to as the T2-shine through artifacts. In order to quantify the diffusion process regardless of the T1 and T2 relaxation effects, the Apparent Diffusion Coefficient (ADC) maps are derived using the Stejskal-Tanner equations:

$$ADC = \frac{-1}{(b_0 - b)} ln\left(\frac{S}{S_0}\right)$$

where S_0 is the signal intensity obtained with b_0=*0* s/mm^2 and S is the signal intensity with $b \neq 0$ [38]. Thus scans with different b-values are needed to derive the above map. Diffusion in physics, is defined as 1/3 times the product of the medial velocity times the mean free path. The unit for diffusion is area per time. The b-value is inversely proportional to the diffusion coefficients (ADC). Hence, the unit of b-value comes out to be time per area. [**?**]. As seen from Figure 2.1, the ADC map shows reduced diffusion in the area of stroke and appears dark relative to the normal tissue. Significantly bright region on a DWI scan accompanied with low intensity value on the ADC map is an indicator of the stroke region in the data.

2.3 Proposed Multi-Stage Pipeline

2.3.1 Argument for Design of Multi-Staged Pipeline

The stroke lesions in the DWI scan appear as bright hyper-intense regions, however with variable sizes and observed intensity inhomogeneity across the scans as evident from Figure 2.1. An intensity based segmentation method alone will not be able to reject the falsely segmented regions due to the presence of *shine-through* artifacts that mimic the stroke appearance. An example of shine-through artifact is shown in Figure 2.3. Also, the intensity based segmentation method will fail to accurately capture the small-sized lesions in the data due to low resolution and poor SNR of the DWI scans. Hence, a multi-stage pipeline where the true lesion locations are detected in *detection* stage and the detected true lesions are accurately segmented in the *segmentation* stage is proposed. Such a pipeline enables us to perform the task of detecting the bright hyper-intense regions in the data separately.

Clinical studies have proven the usefulness of imaging the DWI scans with higher b-value. High sensitivity is achieved for the task of stroke detection on DWI scans with higher b-value, however at the cost of specificity. In order to increase the specificity by reducing the number of false detections, information across the DWI scans with higher and lower b-values can be utilized along with the complementary information provided by the ADC maps. After detecting the set of true lesions in the data, the segmentation stage can improve upon the boundary of the detected lesions and thus obtain accurately segmented stroke lesions in the data. Another advantage of a multi-stage pipeline is that the windowing operation can be performed in a separate *pre-processing* stage. This serves the purpose of enhancing the contrast of the lesions in the DWI data which aids their segmentation as well as helps the experts in manual diagnosis.

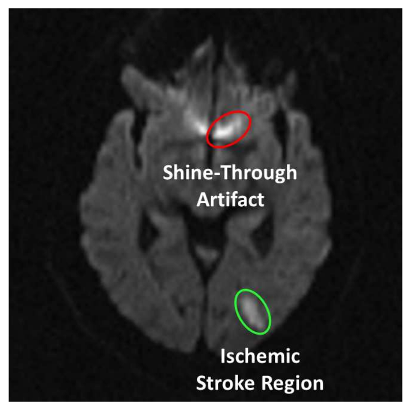

Figure 2.3: A shine-through artifact and a ischemic stroke region as seen on a DWI scan. The shine-through artifact appears similar to the stroke region.

2.3.2 Pre-processing

2.3.2.1 Windowing Operation

Windowing is the process of the contrast stretching where a given range of intensity values (large or small) is extended via a gray-level transformation. A given window setting is characterized by the window level and the width that determines the overall brightness and contrast of the transformed image.

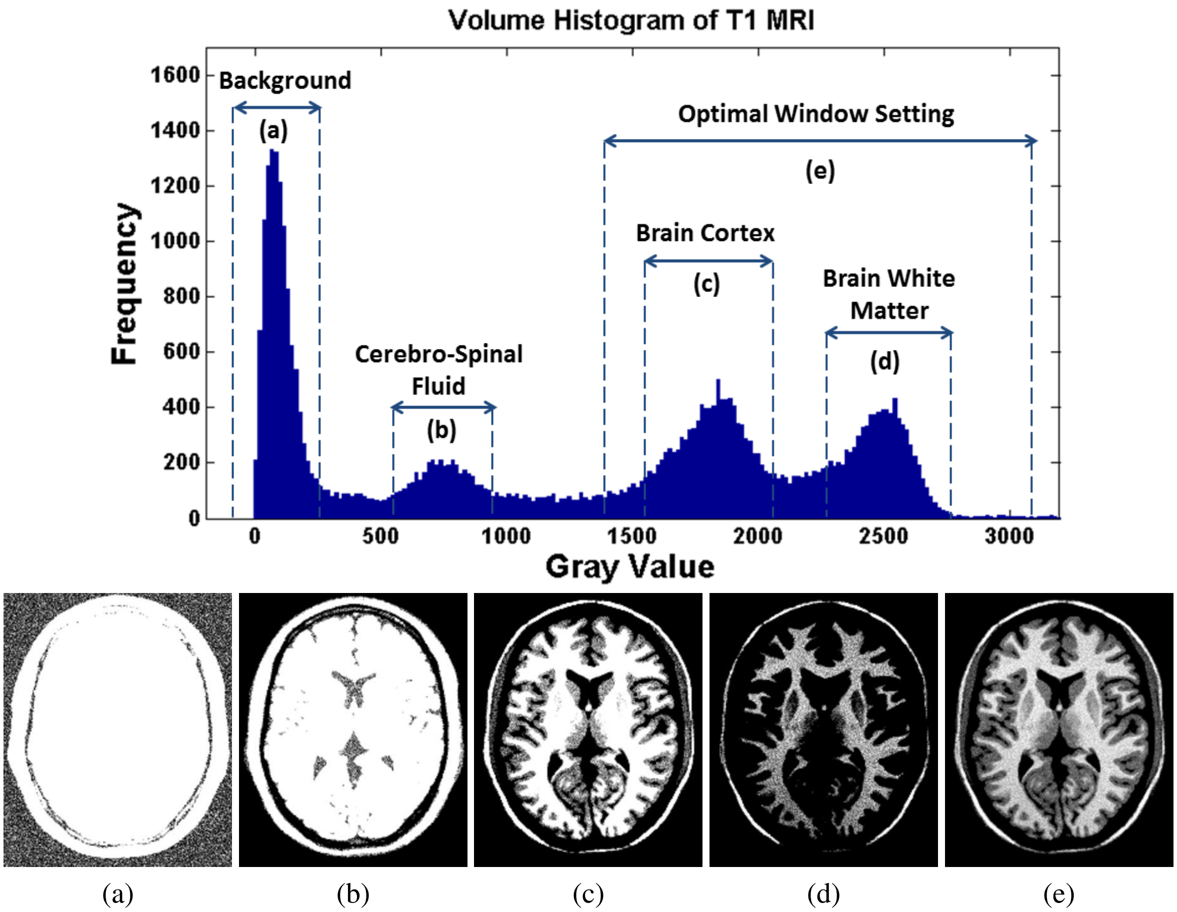

Figure 2.4: Histogram of the T1 brain MRI data. The different peaks in the histogram correspond to the different tissues and regions in the data as shown by the labels. The corresponding scans after windowing are as shown. The different regions can be distinctly seen in the windowed scans.

Window level is the intensity value at the centre of the window and the window width is the range of intensity values around the window level. The window parameters can be varied to generate multiple views of the same raw data based on the contrast differences between the different regions in the data.

2.3.2.2 Need of Windowing on Medical Data

Medical images are typically encoded in 12 or 16 bits and thus the dynamic range of the image intensities is high. The entire range cannot be displayed at once on a standard 8-bit display, albeit with the high information content. When viewing the medical data on a standard 8-bit display, a simple technique would be to compress the entire dynamic range to fit the display range which would result in a low contrast image thus affecting the diagnosis. The high dynamic range also poses a problem to the image processing techniques those are dependent on the subtle intensity variations in the data which might be lost in the high dynamic range. Thus, a contrast enhancement image processing technique is essential to address these issues. Instead of displaying the entire intensity range, a part of the range is displayed utilizing the windowing operation. An example that demonstrates the strength of windowing operation in intelligently viewing T1 MRI data of the brain is shown in Figure 2.4. In doing so, a linear transform is desired which preserves the relative contrast variations in the data while enhancing the data since a non-linear transform may alter the relative contrast variations between different tissues which can lead to false diagnosis. Hence the windowing operation is used as preprocessing step before the medical data is analysed.

2.3.2.3 Need of Windowing on DWI Data

The DWI scan is a measure of the microscopic random motion of the water molecules inside the brain. DWI acquisition is done using the standard echo-planar imaging (EPI) technique which is susceptible to T2 shine-through artifacts. The acquisition process induces a trade-off between signal-to-noise ratio (SNR), time and resolution of the acquired image. Since the acquisition time of DWI scan is very low ($<$1 min), the resolution as well as the signal-to-noise ratio are heavily compromised. Low resolution and noisy data poses a problem in the identification of the ischemic changes and subtle signs of stroke. With the increase in b-value, the data becomes increasingly noisy and while the detectability of the lesions might be improved, extent of the lesions is difficult to judge. Also, varying the b-value generates different sequences with varied contrast for the same tissue.

Identifying the different regions (normal tissue vs abnormal tissue) and boundaries is a necessary and a challenging task for the accurate diagnosis of the DWI scans. Low resolution, multiple artifacts, partial volume averaging, intensity inhomogeneity and varied tissue contrast of the DWI scan make it difficult to visually interpret the results. The results of detection and segmentation are also dependant on these factors and they significantly affects the accuracy of both the tasks. Thus, a preprocessing step which addresses some of these issues and enhances the contrast is essential before diagnosis. Global contrast enhancement may result in loss of local contrast thereby hindering the detectability of small sized lesions and their boundaries in DWI. Thus, windowing operation which enhances the local contrast through a linear transformation and suppresses the noise in the DWI scan is used to enhance the DWI data.

2.3.3 Automatic Windowing Method

An automatic windowing approach is proposed for pre-processing the b2000 and b1000 data for improving the local contrast and definition of the lesions while suppressing noise. Another motivation for proposing the windowing approach is to assist the radiologists in visual analysis of the DWI data for stroke regions. The proposed windowing approach enhances the contrast of the DWI data relative to the stroke lesions present in the data. The method searches for the window setting that maximizes the contrast of the stroke lesions present in the data. It better defines the stroke lesions and thus aids the visual analysis by the experts as well as the automated segmentation.

2.3.4 Detection of Stroke Lesions

Our objective is to accurately detect and segment the stroke lesions. The b2000 data with high sensitivity for stroke is suitable for finding candidate locations. However, due to reduced SNR, relying only on b2000 data can lead to a high number of false positives (FP). The b1000 (with low anisotropy effects) and the ADC (impervious to shine-through artifacts) are appropriate to help reject these FPs. Accordingly, our strategy is to leverage the b2000 data to find candidate lesions and use the ADC and b1000 data to reject FPs.

2.3.4.1 Candidate Selection

The candidate selection stage is based on simple observations and domain knowledge to find an optimal intensity threshold to find the set of candidate stroke lesions in the data. We bank on the property of the stroke lesions to appear as hyper-intense regions in the DWI scan which are typically brighter than the normal brain tissue. The other observation that we make in finding the threshold is that the volume of the brain is much larger as compared to the volume of the stroke region. Combining these two observations we find the optimal intensity threshold from the volume histogram of the given DWI scan. The details of method are explained in Section 3.3.2.

2.3.4.2 Candidate Refinement

In order to refine the set of candidate lesions to obtain the *true* candidates, we perform a candidate refinement stage again utilizing the domain knowledge of the acquisition process for DWI scans. False candidates that mimic the appearance of stroke lesions in the data arise due to artifacts (inherent to the acquisition process) or due to anisotropy effects (caused by increasing the b-value). Thus, utilizing the ADC maps which quantify the diffusion process regardless of the artifacts and integrating the information from multiple b-value scans, we address the false candidates and obtain the set of *true* candidate lesions. The details of the method are mentioned in Section 4.3.3

2.3.5 Stroke Segmentation

Detection of candidate pixels is a relatively easy task compared to their *accurate* segmentation. DWI acquisition is done using the standard echo-planar imaging (EPI) technique which compromises the resolution as well as the SNR of acquired scans and affects the precision with which *subtle* lesions can be detected. Hence, contrast enhancement of the lesions prior to segmentation is required. An automatic windowing-based technique was designed for this purpose. Stroke lesions appear bright in DWI but are inhomogeneous, with complex shapes and observed intensity variation. Hence, an active contour based approach is deemed appropriate for segmentation of the stroke lesions. We propose a modification to the standard Chan-Vese model for active contours [9] to better segment the stroke lesions in the data. The details of the proposed modification are explained in Section 4.4.3.

2.4 Discussion

DWI is an inherently noisy data with multiple contrast for the same tissue. The nature of the appearance of the stroke lesions in the DWI data is ambiguous. Imaging with higher b-values provides a better definition of the stroke lesion which combined with the complementary information from ADC maps gives a significant indicator of the regions of stroke in the data. The different resources provide different information about the stroke and other artifacts in the data and hence demand a clever approach for its integration to characterize stroke lesions. A multi-staged framework with lesion detection and segmentation enables us to address the false positives in the data that mimic the stroke lesions at the detection stage and allows for segmentation of only the true stroke lesions.

With this motivation, we propose a multi-stage pipeline for stroke detection and segmentation as shown in Figure 2.2. The true candidate lesions are obtained in the detection stage by utilizing information from multiple resources (b1000 and b2000 DWI scans and the corresponding ADC maps). A contrast enhancement scheme is proposed to improve the contrast of the DWI scans relative to the stroke lesions present in the data. The segmentation stage utilizes the b2000 DWI scan and fuses the complimentary information obtained from the ADC maps to perform an accurate segmentation of the stroke lesions. The segmentation method thus employs a simultaneous multi-modal approach to define the detected stroke lesions in the data. Following chapters give insight into the concept and implementation of the proposed approaches. Extensive results are provided for validation and a detailed analysis of the results is reported to support the claims proposed above.

Chapter 3

Automatic and Adaptive Windowing Technique

3.1 Introduction

During stroke analysis, the clinical practice is to conduct a fast DWI scan (<1 min) to gain a quick assessment to enable further detailed and accurate diagnosis [12]. Thus, the resultant scan of the DWI acquired using the EPI technique has poor SNR and low resolution due to a short time of acquisition. This affects the detectability of small stroke lesions in the data. On the other hand, in order to achieve accurate segmentation results, a pre-processing stage to enhance the contrast of the data is necessary. The stroke lesions in the data are inhomogeneous with complex shapes. The different lesions in the data show intensity variations across the volume and hence a contrast enhancement scheme is necessary to improve the lesion definition which aids the segmentation process. In this chapter, we introduce a novel contrast enhancement scheme which automatically and adaptively determines the window settings that enhances the contrast of the DWI data relative to the ischemic lesions. The details of the method are described further in this chapter.

3.2 Brief Review of Existing Methods for Processing MRI/DWI

Visibility of abnormalities in images is key to diagnosis and can be improved via a contrast enhancement technique or windowing. At the clinical level, radiologists routinely adjust the window parameters (width and level) to obtain the best overall contrast and brightness before arriving at a diagnosis. This is partly to adapt to their display device and partly tailored to an abnormality of interest. An optimal window setting for DWI, was manually determined for Hypoxic-ischemic encephalopathy and shown to improve diagnosis across patients and scanners [29]. Semi-automated methods have also been utilized towards standardising the display across patients and scanners [37]. Automated methods for determining the window parameters have aimed at global contrast enhancement. Techniques using spatial, anatomical and histogram information [6] as well as pseudo colorisation (of segmented results) [30] have been proposed. In the latter case, different tissue classes for T2 weighted MR images are identified from the histogram and the pseudo-colorisation is done using fuzzy membership functions. The problem of over-

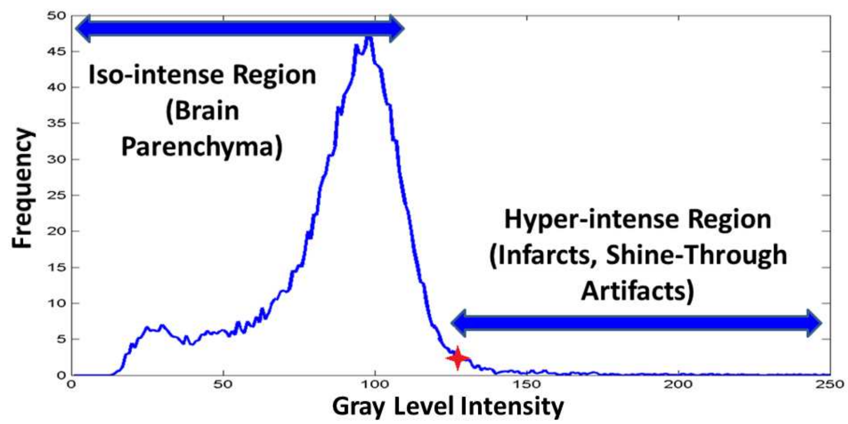

Figure 3.1: Regions shown on histogram of a DWI brain volume with background suppressed. Knee-point beyond which infarcts and shine-through artifacts lie, shown in red.

enhancement and high complexity of adaptive-histogram equalization is overcome by proposing a local bi-histogram equalization technique in [42] for medical images. A wavelet transform-based approach [41] utilizes a linear function for combining the transform coefficients across scales after thresholding. Alternately, a histogram based method [22], incorporating the gradient and intensity information serves to enhance the white matter lesions while suppressing the background in FLAIR MRI.

Global contrast enhancement may result in loss of local contrast thereby hindering the detectability of small sized lesions and their boundaries in DWI. Such techniques can also result in a non-linear transformation which will change the relative contrast between different tissues which is undesirable. A linear transform which preserves the relative contrast variations while enhancing the data is preferable.

The discrimination of subtle ischemic lesions can be confounded by presence of artifacts (for example, susceptibility-related shine through, coil sensitivity, T2 shine through) and acquisition related changes (b1000/b2000) [24]. The practice of acquiring DWI scans of different b-values produce varied contrast for the same brain tissue. The intent is to help improve the discriminability of ischemic lesions in the data while preserving the relative contrast among the tissues. Proposing a contrast enhancement technique helps to serve two purposes: (i) improving the lesion definition to aid the segmentation task and (ii) assisting the clinicians by providing a standard across data from different scanners and acquisition protocols. With this motivation we propose the contrast enhancement scheme for processing DWI data with respect to the ischemic stroke lesions in the data.

3.3 Method for Auto-Windowing

3.3.1 Concept

The auto-windowing problem requires finding two parameters, the optimum window level l_o and width w_o. Since the goal is to improve the discriminability of the ischemic lesions, an approach which achieves local rather than global contrast enhancement is appropriate. Accordingly, we formulate the problem as finding the window setting that maximizes the local contrast for the lesions in a given dataset. Thus, the first step in our approach is to do a coarse segmentation of the lesions from the given DWI dataset. Next, the local contrast is measured for a set of window parameters. The desired *best* window is the one that yields maximum contrast for the lesion(s) relative to the local background. In our work we choose the Contrast-to-Noise Ratio (CNR) as the metric to characterise the local contrast. We now present the proposed auto-windowing method in detail.

3.3.2 Coarse Segmentation

We start with the following observations. In the case of an acute stroke,

- Stroke volume $\ll$ Brain volume.
- The infarct appears brighter than the brain tissue.

The first observation is intuitive and the second one is a property of the DWI scan. Let H_v be the volume histogram of the given DWI volume obtained after masking out the background in the image. From our observations the following conclusion can be made: pixels belonging to lesions will give rise to short peaks at the higher end of H_v. This is illustrated in Figure 3.1. Hence, a simple threshold set at the knee-point after the global maximum in H_v can help select the desired candidates. It is possible to employ a non-linear transformation to find this knee-point accurately, however, a rough method will suffice.

The knee-point is determined by a function which minimizes the error between two line fits which operates as follows: Let G_{max} be the global maximum in H_v. The function iteratively finds a bisection point along the curve after G_{max}. At every iteration, the bisection point divides the curve into two sets of points - curve points lying to the left and to the right of the bisection point. Two lines are fit originating from the bisection point to these set of curve points. The bisection point which minimizes the sum of errors for the two line fits is determined as the knee-point. Figure 3.2 illustrates the two line fits with minimum error at the knee-point.

The given DWI volume data is thresholded at the knee-point and all the pixels having intensities greater than the knee-point are retained. A connected component analysis on these pixels yields a set of coarsely segmented candidate lesions. Connected components with a size less than 5% of the image matrix size were ignored. Sample results of the proposed method are shown in Figure 3.3. As seen from Figure 3.1 the gross anatomy and the intensity distribution of the brain in the DWI scans is relatively similar and hence this method correctly identifies the threshold on all the DWI datasets. The CNR plots for the obtained set of candidate lesions are generated as described in the next section.

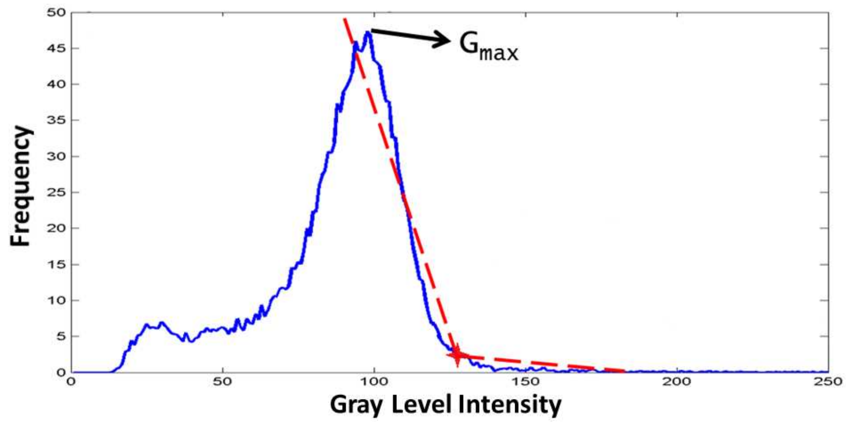

Figure 3.2: Knee-point (shown as a red star), global maximum G_{max} and the corresponding line fits shown on the volume histogram of the brain with the background suppressed.

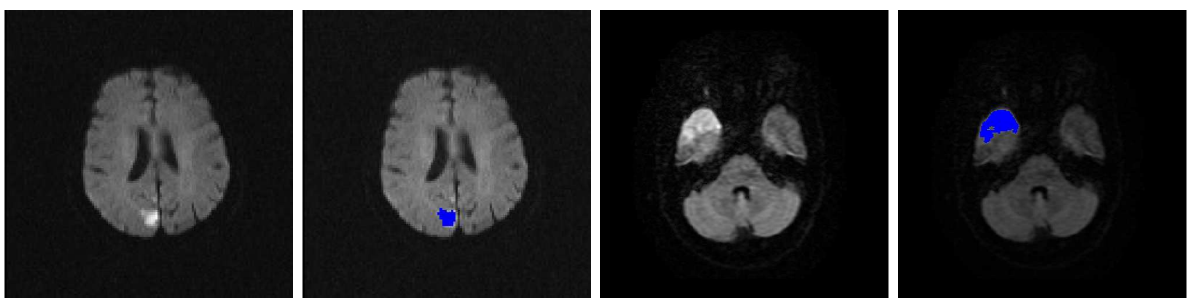

(a) (b) (c) (d)

Figure 3.3: Results of Coarse Segmentation on two slices. (a),(c) are the original images while (b),(d) are the corresponding pseudo colored images where the segmented lesions are shown in blue.

3.3.3 Generation of CNR plots

For each of the candidate lesions, the CNR is computed as:

$$CNR = \frac{\mu_c - \mu_b}{\sqrt{\left(\sigma_c^2 + \sigma_b^2\right)/2}}$$

where, μ_x and σ_x are the mean and standard deviation of the intensity of region *x*, respectively; *c* denotes core region; *b* denotes background. The candidate lesion is considered as the core region and the surrounding normal brain tissue in a bounding box (with a 3 pixel margin) is considered as the background region. The 'normal' tissue is characterised by ADC values in the following range: $[0.6 - 1.15] \times 10^{-3} mm^2/s$ [38]. The ADC maps are referred in order to estimate the background cerebral white matter since it might be the case that the lesion is present at the boundary of CSF region or the brain. We don't want to bias the CNR values by suppressing the mean of the background region. Hence only the cerebral white matter in the bounding box is considered as background which is found using the ADC maps.

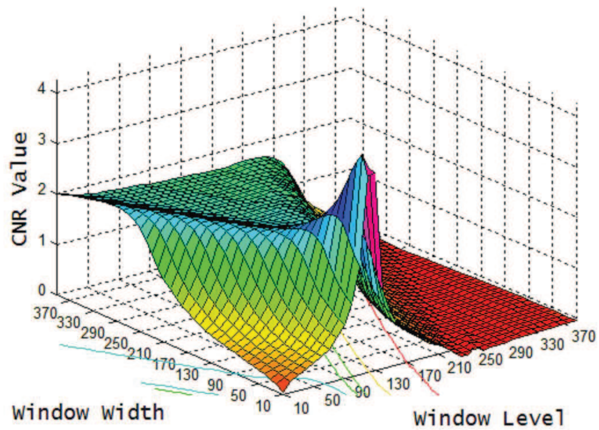

(a)

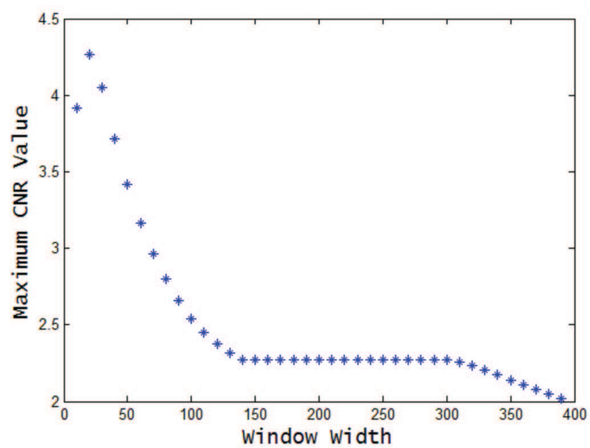

(b)

Figure 3.4: (a) The CNR surface plot obtained with different window parameters (b) Maximum CNR values for different window widths.

Two plots are generated for each volume as shown in Figure 3.4. Figure 3.4(a) is the plot of $CNR(l, w)$ while Figure 3.4(b) is the plot of $max\,(CNR(w))$. The interval $[1, N]$, with N being the maximum intensity in the data, was sampled to generate these plots.

$$\text{l} = n\Delta l \quad ; \quad n = 1, 2, \ldots \text{N}$$
$$\text{w} = m\Delta w \quad ; \quad m = 1, 2, \ldots \text{N}$$

In our implementation, the sampling intervals (Δl and Δw) were fixed at 10. Experiments were done to test the effect of varying the sampling interval on l_o and w_o. A trade-off has been observed between consistency in the obtained window parameters and the computational time with the increase in sampling interval.

The desired optimum level l_o is found from $CNR(l, w)$ and is taken to be the value of l corresponding to the highest CNR value. The desired optimum width w_o is chosen such that the variation in $max\,(CNR(w))$ is below a fixed threshold. As seen from Figure 3.4(a), $l_o = 120$ and from Figure 3.4(b), $w_o = 140$.

Since contrast is a subjective notion the choice of optimal window parameters were made with the following reasoning: Let g_c and g_b denote the gray values of the core and background respectively, for an infarct. Consider the case where $l = g_c$. In this case, the CNR will have a unique peak for this window level, say CNR_p, which will correspond to the smallest w. This can also be observed from Figure 3.4(a). Whereas, if $l < g_c$, the visibility of the infarct reduces and the background starts dominating. Beyond some w, the CNR variation is minimal as the lesion is no longer visible. Consequently, CNR will still attain a maximum ($< CNR_p$), for some w. Since our aim is to enhance the contrast of the lesions, the width value, above which the contrast of the lesions is not affected significantly, is chosen as the desired w_o.

The proposed method is validated through two different means (i) quantitative and qualitative assessment of lesion contrast improvement (ii) perception study analysis with experts. The validation of the results is presented in the further sections.

3.4 Experimental Analysis and Results

The algorithm was tested on the collected datasets and extensive evaluation of the obtained results was done. The evaluation aimed at determining the effectiveness of the proposed auto-windowing method across the following independent parameters: multiple scanners and multiple diffusion weighting (b1000 and b2000). The results were reported on two different methods of assessments - a mirror region of interest analysis and the contrast improvement ratio.

3.4.1 Materials Used

24 DWI volumes of confirmed stroke patients were collected from two local hospitals which had different types of scanners and used different methods of data acquisition. The different b-value data are acquired sequentially on Scanner-1 and simultaneously in Scanner-2. The ADC maps from Scanner-1 were independently generated for both the b1000 and b2000 data using the Stejskal-Tanner equations: *ADC*=$-(1/b)ln(S/S_0)$, where S_0 is the signal intensity with gradient factor *b=0* s/mm^2 and S is the signal intensity with gradient factor *b=1000 or 2000* s/mm^2 [38]. The full data description is provided in Table 3.1.

3.4.2 Mirror Region of Interest Analysis

The mirror region of interest analysis (MRA) was done to validate the improvement in the contrast of the lesions relative to the anatomically similar background brain tissue as represented by the mirrored region. This was achieved by flipping the lesion around the mid-line of the brain and the obtaining the

Table 3.1: Data Description of the DWI Volumes Collected from the Two Local Hospitals With Different Types of Scanners and Different Acquisition Protocols.

Scanner	Data-sets	Acquired Data	Voxel Size	Matrix Size/Pixel Depth (PD)
Scanner-1	8	b=0, b=1000, b=2000, ADC = Post Acquisition (Sequential)	0.98×0.98 ×6.32mm	256×256×22 /PD=16 bits
Scanner-2	16	b=0, b=1000, b=2000, ADC = During Acquisition (Simultaneous)	1.95×1.95 ×7.28mm	128×128×20 /PD=12 bits

corresponding mirror region in the contra-lateral hemisphere. The contrast of the lesion relative to this mirror region and the percentage improvement in the contrast were measured as,

$$C_M = \frac{|\sum_i^n \mu_i - \sum_i^n \tilde{\mu}_i|}{\sum_i^n \tilde{\mu}_i} \quad ; \quad C_{MI} = 100 \times \frac{(C_{M_W} - C_{M_{NW}})}{C_{M_{NW}}};$$

where, μ and $\tilde{\mu}$ are the mean intensity values of a lesion and its mirrored region respectively and n is the number of lesions. The C_M values were computed only for candidate lesions that showed true lesion characteristics determined from ADC maps. Candidates in the specified range of ADC values ($[0.15 - 0.6] \times 10^{-3} mm^2/s$) for acute infarct regions were used. The improvement in the C_M values is quantified as a percentage by C_{MI} defined above. Here, C_{M_W} and $C_{M_{NW}}$ are the C_M values for windowed and non-windowed data respectively. This metric, in essence, captures the improvement in the lesion contrast, relative to the global background brain tissue as represented by the mirrored region. For a given dataset, the mid-line was detected manually.

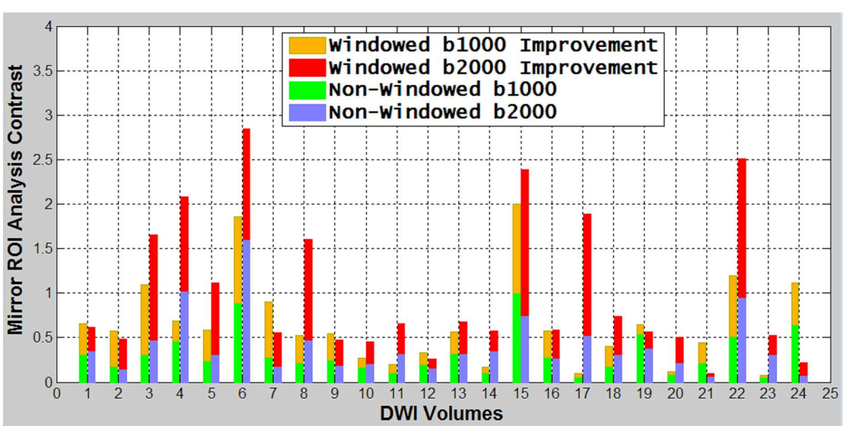

Figure 3.5: Results of Miror ROI Analysis

3.4.3 Contrast Improvement Ratio Analysis

The contrast improvement ratio (C_{IR})[22] was computed to validate the improvement in the local contrast of the lesion relative to the local background. The C_{IR} is defined as,

$$C_{IR} = 100 \times \frac{\sum_i^n \mid c_i - \hat{c}_i \mid^2}{\sum_i^n c_i} \quad ; \quad c_l = \frac{|\mu_c - \mu_b|}{|\mu_c + \mu_b|}$$

where, c and $\hat{c}$ represent the local contrast without and with windowing respectively and n is the number of lesions. The local contrast c_l is defined based on the mean values of the lesion (μ_c) and its local background (μ_b). The normal brain tissue present in the bounding box with a 3 pixel margin around the lesion is used to define the lesion's local background. The C_{IR} values are computed only for true candidates which were determined as described earlier.

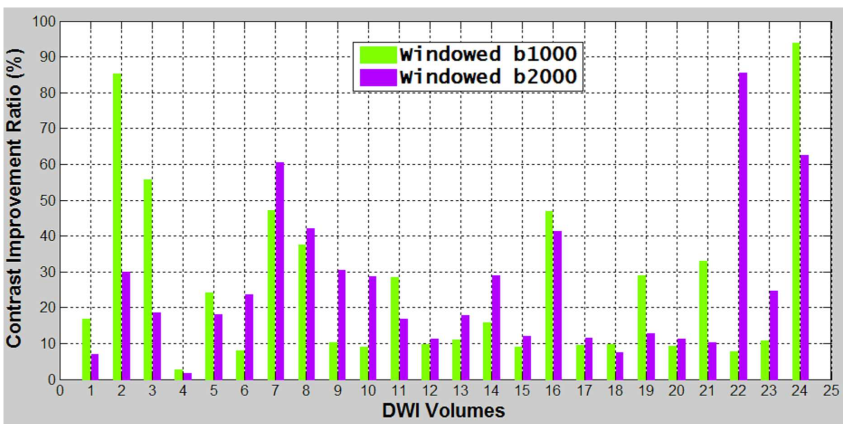

Figure 3.6: Result of Contrast Improvement Ratio(%) Analysis

3.4.4 Analysis of Results

The C_M values for data with and without auto-windowing are plotted in Figure 3.5 for both b1000 and b2000 datasets. The average C_{MI} values were found to be (34.35%, 59.71%) for (b1000, b2000) respectively. We note from Figure 3.5, that the C_M values are high for both windowed and non-windowed b2000 data in most of the cases. Such a trend is to be expected since b2000 offers higher contrast of the lesions relative to the b1000 data [35]. In our dataset, it was found that there was only one volume where the lesions occurred in contra-lateral locations in the same slice (shown in Figure 3.8(u)).

The results of quantitative evaluation of C_{IR} are presented in Figure 3.6. The average values of C_{IR} were found to be (25.82%, 25.59%) for (b1000, b2000) respectively. As seen from Figure 3.6, there is a minimum improvement of 10% in the C_{IR} values across volumes with the exception of the 4^{th} volume. This volume had only one small lesion (shown in Figure 3.8(e)) causing the negligible improvement in C_{IR}. There was a significant improvement in C_{IR} for b1000 data as compared to the b2000 data for the 2^{nd}, 3^{rd} and 24^{th} volumes. These had medium sized lesions of with poor contrast in the b1000 data which improved with an increase in b-value (b2000). Consequently, the C_{IR} values are higher for b1000 cases. There is significant improvement in the C_{IR} value for the 22^{nd} volume for the b2000 data because the b1000 acquisition is highly noisy and the contrast variation in the tissues is highly distorted due to presence of artifacts. In sum, the size of the lesions has a bearing on the quantitative results. With an increase in lesion size the variation in the intensity within the core region also increases which affects the C_{IR}.

Table 3.2: Quantitative Comparison of Results Across Scanners. Mean values of C_{MI} and C_{IR} computed across the scanners.

Scanner	C_{MI}		C_{IR}	
	b1000	b2000	b1000	b2000
Scanner-1	23.59%	53.51%	21.39%	25.13%
Scanner-2	39.73%	62.82%	34.67%	25.82%

The mean values of C_{MI} and C_{IR} were computed across the scanner and the values were found to be as reported in Table 3.2. From the results we can infer that windowing is more effective to data obtained from scanner-2 relative to scanner-1. The voxel size, matrix size and the pixel depth of the data obtained from scanner-1 is higher relative to that of the scanner-2. Thus, the data from scanner-2 has poorer contrast and noisier relative to data from scanner-1. Hence the improvement in local and the global contrast after windowing as measured by C_{IR} and C_{MI} respectively is more in data from scanner-2 relative to scanner-1.

Overall, the quantitative assessment of the proposed method indicates that the method results in a significant improvement in the contrast of the lesion relative to global brain tissue background *and* relative to the local background. It is also noteworthy that the reported results are obtained over datasets with different acquisition protocols. This demonstrates the robustness of the method.

3.4.5 Gain in Segmentation Accuracy through Windowing

In order to further validate the gain in local contrast and assess the gain which can be expected in segmentation with the proposed windowing approach, the coarse segmentation method as described Section 3.3.2 was used and the results were compared with the ground truth obtained from experts (neuro-radiologists). Sample colour coded segmented results are shown in Figure 3.7. The colour code is as follows: blue, red and green pixels indicate true-positive (TP), false-positive (FP) and false-negative (FN) pixels respectively.

The results show that windowing helps in a) reducing the FPs significantly and b) capturing the true extent of the lesions.

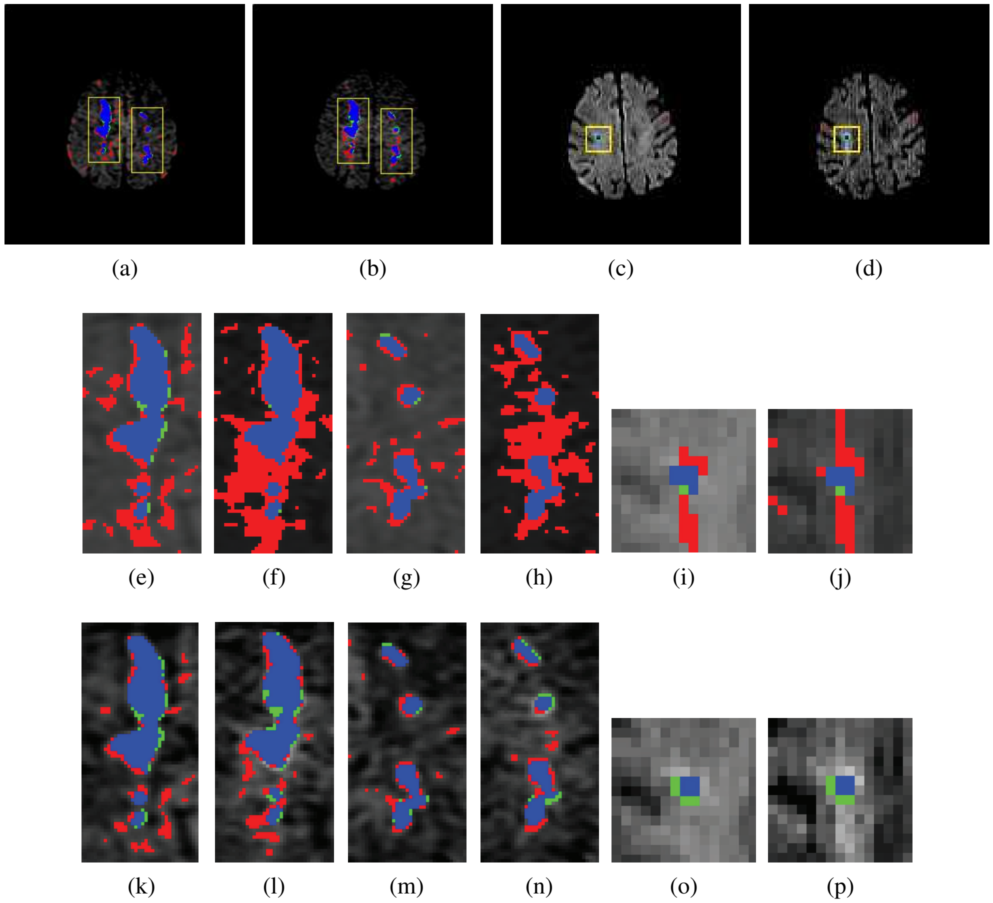

Figure 3.7: Pseudo-colored segmentation results obtained using the coarse segmentation method as described in Section 3.3.2. Corresponding zoomed results on original data (e)-(j) and enhanced data (k)-(p). The color code is as follows - Blue:TP, Red:FP and Green:FN.

3.4.6 Qualitative Results of Windowing

Sample windowed and non-windowed results are shown in Figure 3.8. It can be observed that the detectability and the extent of the lesion boundaries is improved as well as the background noise is suppressed in the auto-windowed results which offers much more discrimination between the lesions and the normal brain tissue.

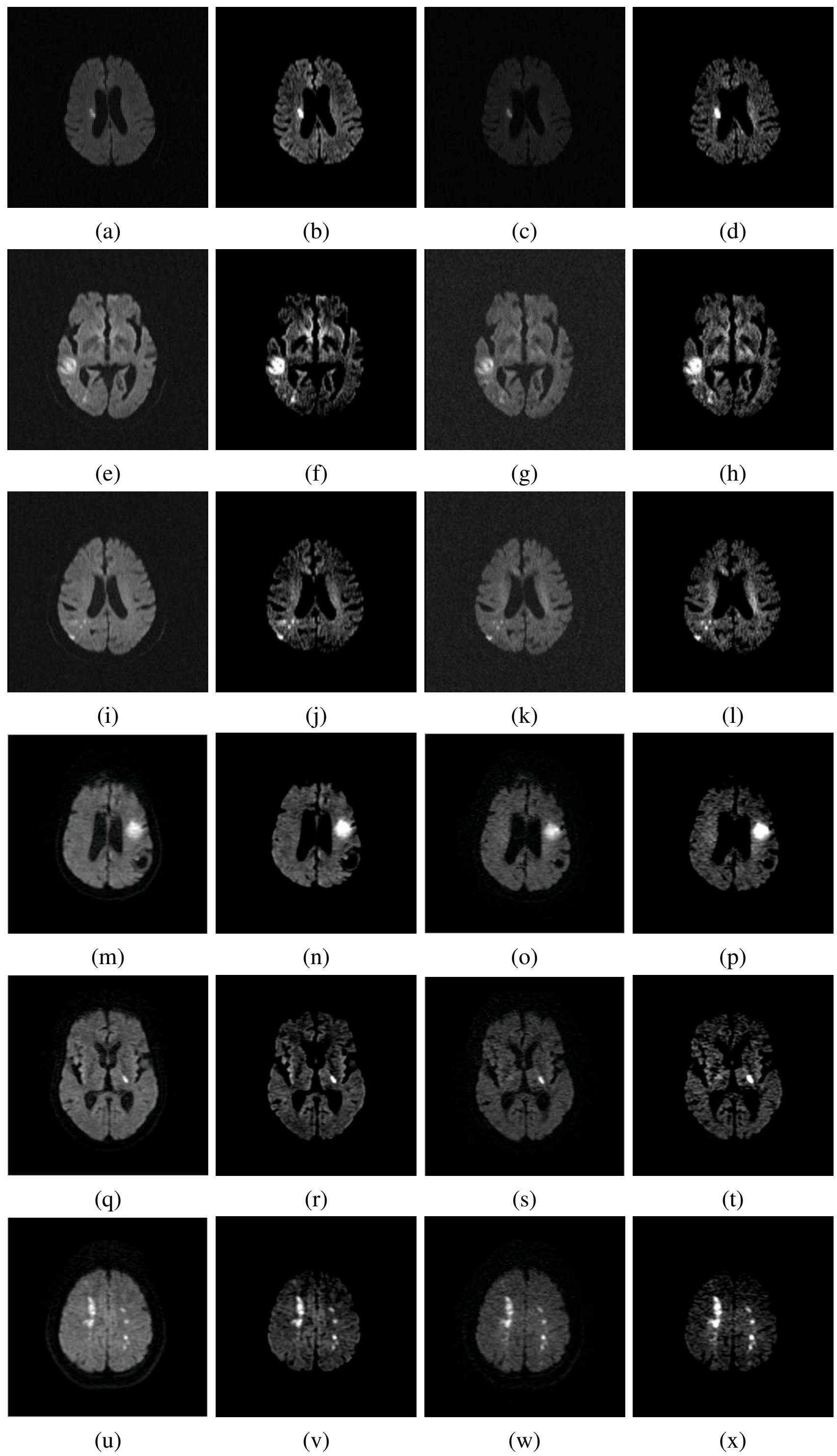

Figure 3.8: Results of windowing on sample images from scanner 1 ((a)-(l)) and scanner 2 ((m)-(x)). First column - original b1000 images; Second column - windowed b1000 images; Third column - b2000 images; Fourth column - windowed b2000 images.

3.5 Perception Study and Results

3.5.1 Introduction

The proposed windowing scheme generates results where the lesions appear bright and can easily be distinguished thus increasing the discriminability of the lesions. However, in order to perform a complete study, a validation of the obtained results from the expert radiologists was required. Hence a perception study was conducted with the hypothesis that the response time in identifying the number of lesions in a presented slice of a DWI dataset is less in case of windowed result as opposed to the case of an original image. The experiment was conducted with different radiologists with varied years of experience. In this section, the proposed experiment that was done as part of the perception study and analysis of the obtained results of the experiment is presented.

3.5.2 Experiment Setting

The objective of the experiment was to note the response time of the radiologists in identifying if the presented slice of DWI is normal or abnormal and if abnormal then noting the number of lesions in the slice to ensure that the all the lesions in the presented slice are captured.

3.5.2.1 Stimuli

The stimuli used for the experiment was a set of windowed and original DWI slices. This set comprised of normal and abnormal slices with different sized lesions, of different b-values and obtained from two different scanners. The categorical distribution of the slices is shown in Figure 3.9.

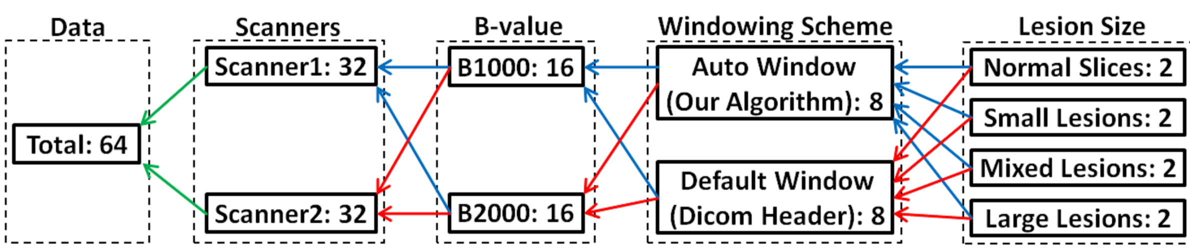

Figure 3.9: Categorical distribution of the stimuli for the perception study. For each sub-category the number of slices is shown.

3.5.2.2 Participants

The participants were radiologists from CARE hospital, Hyderabad [**?**]. There were 8 radiologists with varied years of experience. The radiologists were broadly classified into two groups of *Experts* and *Learners* as shown in table 3.3.

3.5.2.3 Method

For each of the radiologists, the slices were randomly presented and the response time was noted in classifying the presented slice as normal or abnormal (binary output). The number of lesions identified by the radiologist in the presented slice if it was classified as abnormal was also noted.

3.5.2.4 Experiment Environment

The response times of the radiologists were accurately noted using the DirectRT [20] software which is designed for cognitive and perception tasks that require millisecond precision. The experiment was set up in the hospital environment on the monitor regularly used by the radiologists for analysing patient data in order to avoid introducing bias in the measured response times due to different monitor settings (resolution, contrast, brightness settings). The participants were presented with few samples slices to get them acquainted with the functioning of the software before performing the actual experiment.

3.5.2.5 What is the Significance of Windowing?

Stating the significance of performing the windowing operation from a radiologists' point of view required answers to the following set of questions:

- Is there a significant reduction observed in the mean response times for classification of windowed data against that of the normal data?
- Does the sensitivity and accuracy for detection of lesions in the data improve after windowing?
- Does the windowing introduce any artifacts in the data?

The analysis of the perception study was performed with the motivation to provide answers for the above set of questions. Following section explains the analysis performed in detail to find answers and justify them to the questions raised above.

3.5.3 Analysis of Perception Study

3.5.3.1 Brief Introduction to Statistical Analysis

Statistical analysis is done in order to extrapolate any meaningful information from available data to derive general conclusion. The assumption is that the sample data is randomly picked from a larger population where the aim is to find the distribution of the population. The hypothesis confirms a significant reduction in the response times of the windowed DWI slices as compared to those of the non-windowed DWI slices. To validate the hypothesis, it is sufficient to prove that the response times obtained for the windowed and the non-windowed data are selected from two different populations.

Table 3.3: Effect of Windowing on Observers with Different Expertise Levels. Results of the Statistical Analysis on the Obtained Response Times for the Different Radiologists.

Category	Radiologist	Years of Experience	Reduction in Mean RT (%)	P-value (t-test Outcome)
Experts	E1	29	17.22	0.000657
	E2	20	14.11	0.019214
	E3	17	11.17	0.000846
Learners	L1	4	15.32	0.010151
	L2	4	14.12	0.014375
	L3	3	11.18	0.025503
	L4	2	8.10	0.015574
	L5	0.6	11.47	0.042163

P-value is defined as the probability of the population means being different when the given sample data have significantly different means. For e.g. given that the sample means are significantly different, a p-value of 0.02 implies that there is 2% chance of observing such a difference in the sample means under the assumption that the population means are identical. Thus, a p-value of 0.02 indicates that it is highly unlikely that the two populations have identical means. We perform the statistical analysis on the obtained response times of the radiologists before and after windowing. The p-values for the windowed and non-windowed data are computed using the standard t-test.

3.5.3.2 Statistical Analysis Using t-Test

The statistical hypothesis testing is done using a t-test. The t-test quantifies the amount of trust to be placed in the sample mean. When comparing two sample means the discrepancy is quantified by the measure known as t-score. It is dependent on the difference in the sample means, the number of observations in the sample sets and the spread of the observations in the sample data sets. For a given study, first the null hypothesis and an alternate hypothesis are stated which are mutually exclusive. The null hypothesis corresponds to the assumption that the population means are identical and the significant difference observed in the sample means is due to random sampling. The null hypothesis in our case is stated as $\mu = m_0$ where μ is the mean of the windowed samples and m_0 is the reference mean of the non-windowed data. The alternate hypothesis in our case is $\mu < m_0$. The next step is to define a significance level to be considered while rejecting the null hypothesis which is nothing but the threshold to be considered for the p-value. The significance level is traditionally set to 0.05. We perform the statistical analysis using the t-test and obtain the p-value. If the obtained p-value is less than the threshold, then we reject the null hypothesis stating that the difference between the means is statistically significant and not a mere coincidence which indicates that the obtained sample datasets are indeed from two different populations.

Table 3.3 gives the results of the t-test performed on the data and the results of the mean reduction in the RT obtained for different radiologists. First, we examine the RT for decision making by an

Table 3.4: Effect of Windowing on Detecting Lesions of Different Sizes. Results of the Size-Based Analysis of the Obtained Response Times for the Different Radiologists.

Category	Radiologist	Percentage Change in RT			
		Small	Mixed	Large	Normal
Experts	E1	-17.85	-30.48	-13.60	+1.22
	E2	-18.47	-2.34	-29.06	+0.45
	E3	-16.24	-23.75	-9.11	+0.26
	Mean	**-17.52**	**-18.86**	**-17.26**	**+0.64**
Learners	L1	-36.43	-22.75	+3.02	-9.10
	L2	-33.14	-16.88	-14.25	+6.04
	L3	-23.33	-25.20	-6.69	-0.43
	L4	-7.50	+6.42	-11.09	-16.56
	L5	+5.63	-16.45	-4.95	-22.72
	Mean	**-18.95**	**-14.97**	**-6.79**	**-8.55**

observer. The t-test was used to ascertain the statistical significance of the obtained results. The p-value listed in Table 3.3 characterizes the significance, with a $p < 0.05$ indicating a high degree of statistical significance. The mean RTs can be seen to be reduced by 14.17% & 12.04% for *Experts* and *Learners* respectively. Thus the analysis strongly contributes to the initial expectation. It is noteworthy that there is no observable trend in the RTs across expertise levels.

Next, we studied the effect of windowing and size of lesions on the RT. The results of such an analysis are presented in Table 3.4. The (-) sign indicates a reduction while a (+) sign indicates increase in RT with windowing. Overall, it is apparent that windowing serves to reduce the RT for the learner group for slices with smaller lesions, more, than mixed or larger ones. Detection of small-sized lesions in the data is crucial and the most difficult task in abnormality detection and hence these results are attractive. In contrast, the reduction in RT does not seem to depend much on the lesion size for the expert group.

An interesting outcome is the trend observed for normal slices across expertise levels. *Experts* took marginally more time to analyse normal slices after windowing whereas the average RT is reduced for the *Learners*. The normal data in the stimuli contained slices with shine-through artifacts. Thus reduction in RT validates the utility of windowing for the *Learners*. The cautious decision making of the *Experts* in ruling out artifacts, enhanced after windowing could possibly lead to the marginal increase in the RT.

The quantitative evaluation of the obtained perception study results is presented in table 3.5. The sensitivity and specificity values for the lesion detection in the presented slices, were calculated utilizing the following parameters.

- True Positive Slice (TPS): Slice for which number of stroke lesions identified is same compared to that in the ground truth.
- False Positive Slice (FPS): Slice for which number of stroke lesions identified is more compared to that in the ground truth.

Table 3.5: Receiver Operator Characteristics Analysis for Preforming the Task of Stroke Detection in the Data.

Category	Radiologist	Sensitivity		Specificity		Precision		Accuracy	
		Before	After	Before	After	Before	After	Before	After
Experts	E1	0.95	0.97	0.67	0.88	0.88	0.96	0.87	0.94
	E2	0.76	0.91	1.00	0.60	1.00	0.83	0.81	0.81
	E3	0.71	0.81	0.55	0.63	0.75	0.81	0.66	0.75
	mean	**0.81**	**0.90**	**0.74**	**0.71**	**0.87**	**0.87**	**0.78**	**0.83**
Learners	L1	0.72	0.76	0.85	0.87	0.94	0.95	0.75	0.78
	L2	0.82	0.95	0.47	0.55	0.63	0.80	0.65	0.81
	L3	0.58	0.67	0.87	0.77	0.93	0.89	0.65	0.69
	L4	0.29	0.52	0.33	0.23	0.33	0.50	0.31	0.41
	L5	0.74	0.81	0.55	0.64	0.81	0.81	0.68	0.75
	mean	**0.63**	**0.74**	**0.61**	**0.61**	**0.73**	**0.79**	**0.61**	**0.69**

- False Negative Slice (FNS): Slice for which number of stroke lesions identified is less compared to that in the ground truth.

- True Negative Slice (TNS): Slice for which no stroke lesion is identified and the ground truth does not contain any stroke lesion.

The mean improvement in the sensitivity, specificity, precision and recall values is 20.21%, 0.2%, 9.42%, 12.34% respectively. These values correlate with our initial expectation. Improvement in the mean sensitivity suggests that the windowing improves the detection of the true-positives (stroke slices) and helps in accurately identifying the stroke lesions in the data. Negligible change in the specificity suggests that windowing does not affect the detection of the normals in the data. A further detailed analysis of the perception study results is presented in the next section.

3.5.3.3 Further Analysis of Detection Results

In order to further validate the usefulness of windowing in detecting normal and abnormal slices, a set of experiments was conducted. The aim of the experiments was to study the trend observed in the results against the experience of the radiologist - if the windowing affected the detection results differently with the experience of the radiologist. The radiologists were categorized into four groups according to their experience as described in table 3.6.

Experiment 1: The experiment aimed at studying the effect of windowing on the response times in detection of abnormal slices. The mean response times for the detection of abnormal slices were plotted for each group. As seen from Figure 3.10, the mean response times before windowing show a decreasing trend with dereasing experience. A similar trend is observed in the mean response times after windowing with the exception of Group D where the response time increases compared to that of Group C. A notable observation is that the windowing significantly reduces the mean response times for Groups

Table 3.6: Categorization of Radiologists into Groups Based on Experience.

Group	Radiologist	Experience
Group A	Expert 1	29 years
Group B	Expert 2	20 years
	Expert 3	17 years
Group C	Learner 1	4 years
	Learner 2	4 years
	Learner 3	3 years
Group D	Learner 4	2 years
	Learner 5	0.6 years

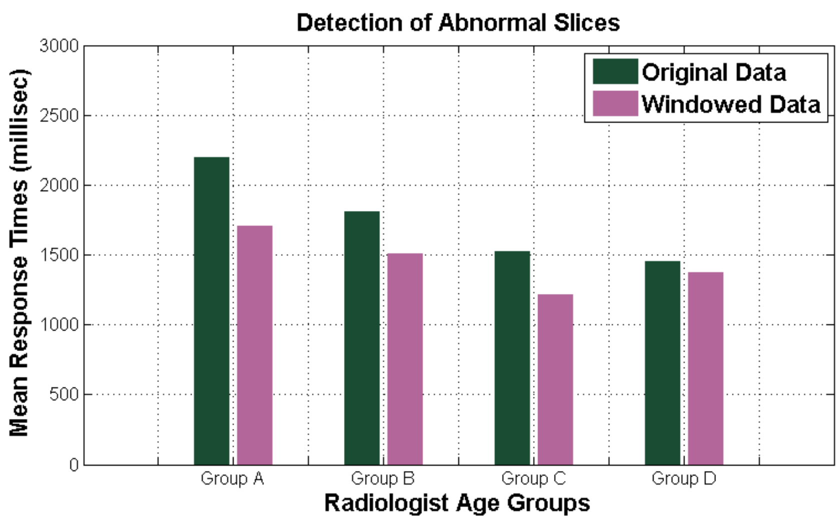

Figure 3.10: Mean response times of radiologist groups for detection of abnormal slices before and after windowing.

A and B which consists of *Expert* radiologists. A significant reduction in the mean response times is also observed in Group C which consists of *Learners* with considerable experience. Negligible reduction in the mean response time is observed for Group D consisting of *Learners* with least experience. From the observations we can deduce that the expert radiologists are assisted most due to windowing in classifying the slices into normal and abnormal. *Expert* radiologists have a high accuracy of detection. Reduction in the response times for the *Expert* radiologists, ensures faster diagnosis which is crucial for treatment of patients with stroke. Hence the significance of the result.

Experiment 2: One of the crucial requirements of any contrast enhancement scheme for medical images is to not introduce any artifacts in the data after processing. The enhancement scheme should benefit the detection of abnormal slices and not affect the detection of the normal slices in the data. Thus, in order to study the effect of windowing on the normal data in the stimuli the following experiment was conducted. As described in *Experiment 1*, the mean response times for detection of normals were noted for all the radiologist groups. The results of this experiment can be seen in Figure 3.11. Negligible

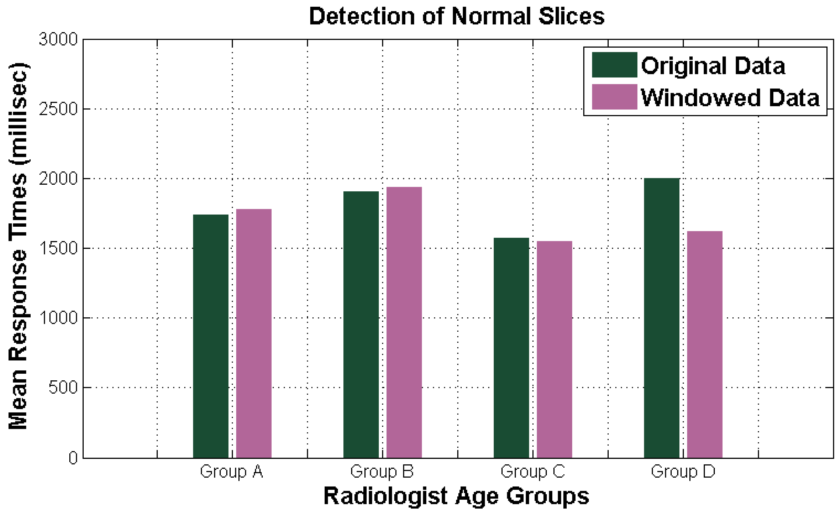

Figure 3.11: Mean response times of radiologist groups for detection of normal slices before and after windowing.

change is observed in the mean response times for the Groups A,B & C while a significant reduction is observed for Group D. No specific trend is observed in the mean response times across the groups before and after windowing. A noteworthy observation made from the plot is that the mean response times of detecting normal slices are **not** affected after windowing.

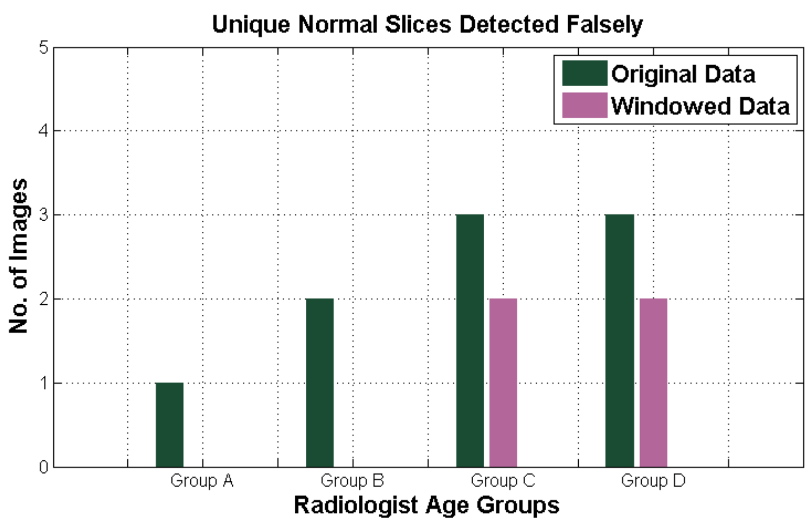

Figure 3.12: Total number of unique normals detected falsely before and after windowing in each radiologist group.

Another experiment was conducted to validate if the windowing aids to improve the detection of normal slices in the data. Among each group, the number of unique normal slices that were falsely detected by the radiologists was plotted as shown in Figure 3.12. The stimuli consisted of 8 normal slices. For Groups A and B consisting of *Expert* radiologists, there are no false detections in the normal data after windowing. For Groups C and D consisting of *Learners*, the falsely detected normals are reduced after windowing. In Groups C and D, no new falsely detected normals were found after windowing. Thus, the windowing significantly helps the *Expert* radiologists in identifying the normal data correctly.

Experiments were also conducted to study if the size of lesions in the data and the number of lesions in the data had a bearing on the mean response times among the groups before and after windowing. However, no significant trend was observed in the plots.

In summary, the significant observations made from the above experiments are

(i) Windowing operation significantly reduces the mean response time for detection of abnormal stroke slices in the data.

(ii) Windowing operation does not affect the mean response time of detecting normals.

(iii) Windowing operation assists the radiologists in identifying normals.

(iv) Windowing operation does not introduce any artifacts in the data.

From these observations we conclude that the windowing operation helps the radiologists significantly in stroke diagnosis and the method is validated from the radiologist's point of view.

3.6 Discussion & Conclusions

A novel automated windowing technique was presented for diffusion weighted MRI. The technique was shown to significantly improve the contrast of ischemic stroke lesions present in the DWI scan. The proposed method is effective for different b-valued DWI scans (b1000 and b2000) and robust to data acquired from different scanners with different acquisition processes. The qualitative and quantitative results reported in this study show promise in the proposed method. Improvement in the lesion definition suggests the effectiveness of the approach as pre-processing step for contrast enhancement in a segmentation framework. The perception study performed with expert radiologists and detailed analysis of the results indicates the effectiveness of the algorithm for clinical usage from the radiologist's point of view. The presented results and the extensive evaluation validates the method and it may play an important role in diagnosis of ischemic stroke in clinical trials.

Chapter 4

Segmentation of Stroke Lesions

4.1 Introduction

One of the most important tasks in image processing is of segmentation. The segmentation task involves labelling the semantically meaningful regions in the given image data. In our case, we try to accurately obtain the boundaries of the stroke lesions in the given DWI data. The segmentation method employed to achieve this task is the active contour framework with a modification that enables the proposed framework to fuse information from multiple sources. The active contour framework is deemed appropriate for the task of segmentation since it is robust to shape and size constraint and the assumption of homogeneity of regions is relaxed in the extended framework. This chapter explains the implementation of the extended Chan-Vese framework [9] for active contours and a detailed analysis of the obtained results is reported. Performance analysis of the proposed framework with other system variants and a leading method in literature shows the superiority of our approach.

4.2 Brief Review of Existing Methods for Stroke Segmentation

Different clinical studies in literature have shown the usefulness of diffusion-weighted imaging with higher b-values. As described earlier, imaging with higher b-value provides better sensitivity to the smallest areas of infarction in the data at the cost of SNR.

Figure 4.1 shows the same slice from two different DWI scans acquired with $b = 1000$ and $b = 2000$. As seen from Figure 4.1, the stroke lesion has improved conspicuity and contrast in the $b2000$ scan relative to the $b1000$ scan. On the other hand, the $b2000$ scan appears noisy as compared to the $b1000$ scan. Thus, the $b2000$ scan provides better detectability and lesion definition relative to the $b1000$ scan at the cost of SNR of the complete scan.

Although imaging with higher b-values is useful, automated methods for stroke detection utilizing the DWI, have been assessed, to date, only on b1000 data. We argue that using multiple b-values may be beneficial for stroke detection and propose a method which exploits the improved lesion conspicuity

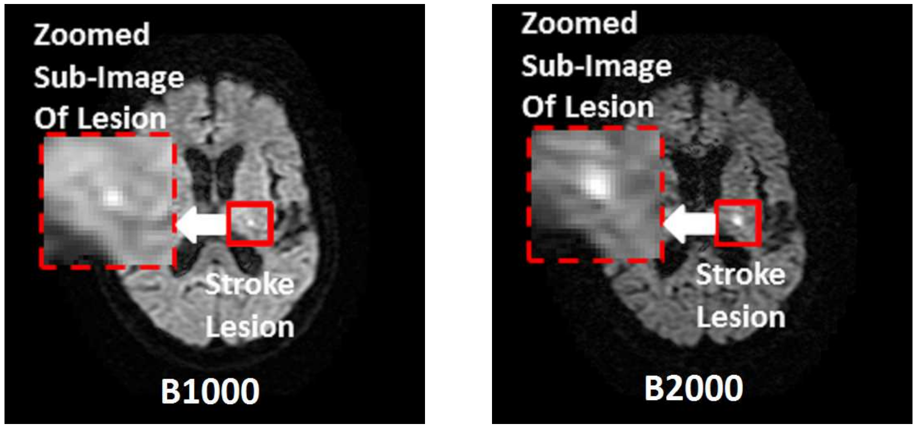

(a) (b)

Figure 4.1: Stroke lesion (marked in red) as seen on (a) b1000 Image and (b) b2000 Image. Zoomed sub-image of the lesion on both the scans reveals improved lesion definition and contrast of the stroke lesion on the b2000 image as compared to the b1000 scan.

to be had with higher b-values with a judicious combination of information from lower b-value scan and the ADC map.

Prior methods for segmenting ischemic lesions in MRI maybe broadly classified into three types - manual, semi-automated and automated. Manual methods for segmentation may provide accurate results for further analysis but are labour intensive and operator-dependant [11].

Semi-automated methods rely on operator intervention in tuning the algorithm parameters or to initialize the algorithm. A semi-automatic adaptive thresholding algorithm utilizing the Markov Random Field framework to model a spatial constraint and the Iterative Conditional Modes method to find a locally optimum solution was proposed in [27] where operator intervention is required in initializing the threshold for segmentation and in post-processing the false-positives. A semi-automatic hybrid method utilizing classical statistics in a deformable models framework utilizing both the intensity-based and the shape-based information to segment and measure the infarct volume in 3-D is proposed [40]. Here, the operator intervention is required in initializing the contours for evolution.

Automated methods have received more attention recently. The automated methods comprise of complex techniques operating on multiple modalities, with multiple stages of data processing as well as simple data-driven histogram-based approaches. A modified unsupervised approach of the Iterative Self-Organizing Data Analysis Technique (ISODATA) using multi-parameter MRI (T1 weighted, T2 weighted, Diffusion weighted, ADC maps) data was implemented in [18]. Here, a multi-dimensional feature space is constructed utilizing the multi-parameter MRI and segmentation is performed by the unsupervised ISODATA clustering method. The tissue clusters are classified by determining the angle between clusters in the feature space. [21] proposed a multi-modal Markov Random Field model operating on T2-MRI, FLAIR-MRI and Diffusion Weighted-MRI sequences simultaneously for segmentation of stroke lesions. A detailed lesion assessment was performed by super-imposing segmented results to the atlas of blood supply territories. In [3], an artificial neural network is trained utilizing multiple MRI sequences (Diffusion-Weighted-MRI, T1-MRI, T2-MRI, and proton density weighted-MRI) to predict the outcome of the ischemic stroke.

Automated, multi-staged methods on single MRI modality have also been proposed. These include a multi-stage unsupervised method which involves pre-processing, calculation of tensor field and measurement of diffusion anisotropy, segmentation of infarction volume using adaptive multi-scale statistical classification [25]. The classification strategy takes into account spatial, gradient, diffusion anisotropy, and contextual information of the original DT-MR images. A partial volume voxel reclassification is employed to make segmentation more accurate by using local parameter information. Identification of the infarct slices through a probabilistic neural network and segmentation of the infarcts using an adaptive Gaussian mixture model has also been reported [7].

In the category of data-driven and histogram based approaches a non-parametric density estimation technique is used in [32] for cerebral infarct segmentation followed by a refinement of the class boundaries using an edge confidence map. Identification of stroke slices, hemisphere and segmentation of stroke regions is achieved in [8] with a divergence measure based on the ratio of intensity probability density functions. A split-merge approach has also been reported for segmenting hyper-intense and hypo-intense brain lesions [36]. The pixels at each split are classified as hyper- or hypo-intense based on a histogram based thresholding technique. In [39], inconsistency between the intensity-based segmentation and the spatial-location-based tissue distribution is measured to identify the infarct lesions. The intensity-based segmentation was performed using the standard fuzzy c-mean algorithm and the spatial location of tissues was provided by prior tissue probability maps.

In summary, stroke lesions appear hyper-intense on DWI and are inhomogeneous, with complex shapes and ambiguous boundaries with observed intensity variation [23] which makes manual segmentation difficult and time consuming. *Early* detection of regions of ischemic stroke (regardless of size and location) is critical for treatment. We argue that a better strategy for accurate stroke detection and segmentation would be to use information from scans acquired with low and high b-values and the ADC maps. We have investigated this idea and propose a novel framework for combining information from b1000, b2000 DWI scans for stroke detection and segmentation.

4.3 Method for Segmentation

4.3.1 Concept

The objective is to accurately detect and segment the stroke lesions. The b2000 data with high sensitivity for stroke is suitable for finding candidate locations, however, will have high number of false positive locations (FP) due to reduced SNR. The b1000 (with low anisotropy effects) and the ADC (impervious to shine-through artifacts) are appropriate to help reject these FPs. An automatic windowing approach is proposed for pre-processing the b2000 data to suppress the noise and improve the local contrast and definition of the lesions. An extended version of the Chan-Vese [9] formulation of active contours is proposed for final segmentation.

4.3.2 Candidate Selection

Given a DWI volume the candidate lesions locations are detected by the method as described in 3.3.2. As illustrated in Figures 3.1 & 3.2, the pixels corresponding to the lesions in the data have gray values that give rise to short peaks at the higher end of the volume histogram. To capture these pixels a threshold is set at the knee-point and the pixels having intensities greater than this threshold are retained. A connected component analysis gives a set of candidate lesions which are refined, as described next, to obtain true lesion locations.

4.3.3 Candidate Refinement

Diffusion takes place in the three dimensional space. Diffusion occurs more along the path of a fibre than perpendicular to it which leads to anisotropy. In order to capture the complete diffusion process, the diffusion gradients are applied in all three orthogonal directions during acquisition. To sensitize the diffusion process regardless of the anisotropy, averaging of the scans obtained in the three orthogonal directions is done. In order to reject false candidates we first rely on the fact that the anisotropy effects increase with the b-value. This point is illustrated in Figure 4.2. Thus, while a true lesion appears bright and has a high local contrast (LC) on both b1000 and b2000 data, the false ones will have different LC in these data. Hence, the ratio of the LC in these two data can serve as a good metric to detect false positives. We investigated this hypothesis and found it to hold true. In order to compute the LC, a bounding box with a 3 pixel margin around every lesion is defined and the LC of the lesion is computed as $LC = \frac{|\mu_c - \mu_b|}{|\mu_c + \mu_b|}$ where, μ_c is mean of the lesion and μ_b is the mean of its local background. The normal background pixels are found by imposing a constraint on the ADC values. ADC of normal tissue pixels are expected to be within $[0.6 - 1.15] \times 10^{-3} mm^2/s$) according to [38]. The ratio of the LCs (b1000:b2000) was thresholded to reject the FPs. This threshold was empirically determined to be 0.6. Lowering the threshold would result in greater number of FPs while increasing it reduced the FPs at cost of small infarcts with poor LC. A value of 0.6 was found to be optimal in all the datasets.

The above LC ratio-based rejection will not be able to reject FPs that arise due to shine-through artifacts since they appear significantly bright on both the b1000 and the b2000 data. Hence, a second stage of rejection is needed. As mentioned earlier, referring to the ADC data is a good choice to address the artifacts. The expected range for ADC values for stroke pixels is $[0.14 - 0.6] \times 10^{-3} mm^2/s$ [38]. Hence, the ADC value of every candidate is checked and all outliers are rejected. After this refinement stage we have a set of potential lesion locations which is passed on to the next stage for lesion segmentation.

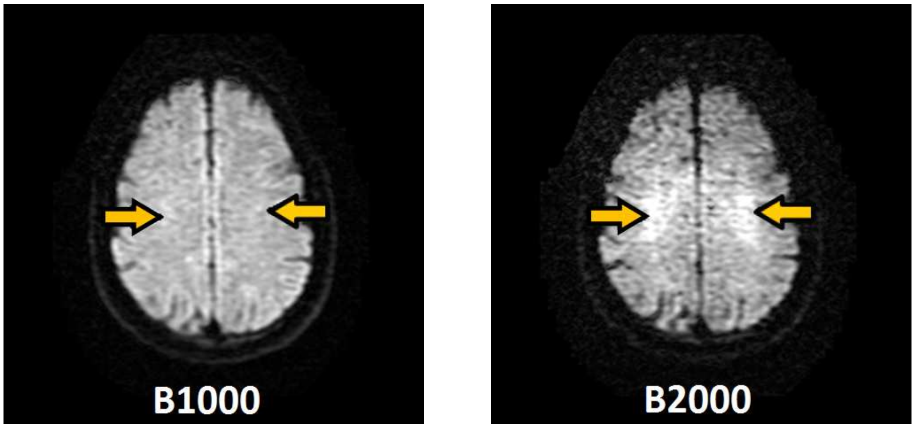

(a) (b)

Figure 4.2: Anisotropy effects increasing (appear brighter) with increasing b-value in areas of white matter tracts as seen on (a) b1000 scan (b) b2000 scan

4.4 Lesion Segmentation

Stroke lesions appear bright in DWI but are inhomogenous (within and across lesions) with complex shapes. Hence, detection of candidate pixels is a relatively easy task compared to *accurate* segmentation. An enhancement of the local contrast of the lesions is therefore a solution to improving the lesion definition. We utilized an automatic windowing-based enhancement as described earlier in Chapter 3.

4.4.1 Automatic Windowing

The low resolution as well as the poor SNR of the acquired DWI scans affects the performance of the image analysis tasks of segmentation which operates on lesion contrast and definition, since subtle intensity changes may get lost. Hence contrast enhancement of the lesions as a preprocessing step is required to improve the results of segmentation.

We utilize the method of auto-windowing as described in Chapter 3. The problem of contrast enhancement is formulated as finding the window setting that maximizes the local contrast for the lesions in a given dataset. The first step in the approach was to perform a coarse segmentation of the lesions from the given DWI dataset to find the lesion cores. This was achieved by utilizing the knee-point calculation method as mentioned earlier in Section 3.3.2. Next, the local contrast, LC, was measured for a set of window parameters. The desired *best* window was the one which yielded maximum LC for the lesion(s) as described in Section 3.3.3. The results of automatic windowing operation showed improvement in both the local and global contrast of the ischemic lesions in the data.

4.4.2 Level Set Based Segmentation

Since the shape and size of the lesions vary widely an active contour based approach is appropriate for segmentation. We chose the Chan-Vese model for active contours [9] which is an energy minimization framework based on the Mumford-Shah functional [33], solved using the level-set method. The objective of the Chan-Vese algorithm is to minimize the energy functional $F(c1, c2, C)$, defined by,

$$\begin{aligned}
&F(c1, c2, C) = \mu \cdot Length(C) + \nu \cdot Area(\omega) \\
&+ \lambda_1 \int_{\omega} |u_0(x, y) - c_1|^2 dxdy + \lambda_2 \int_{\Omega \setminus \bar{\omega}} |u_0(x, y) - c_2|^2 dxdy
\end{aligned} \tag{4.1}$$

where, $\mu \geq 0, \nu \geq 0, \lambda_1, \lambda_2 > 0$ are tuning parameters, Ω is a bounded set in $\mathbb{R}^2$, C is an evolving curve in Ω, $u_0 : \bar{\Omega} \rightarrow \mathbb{R}$ is given image and $\omega \subset \Omega$. ω and $\Omega \setminus \bar{\omega}$ denote the regions inside and outside, respectively, of the evolving curve C. The constants k_1, k_2 are the mean values of u_0 inside C and outside C respectively. The first two (curvature) terms on the right hand side, enforce a smoothing constraint on the curve C while the next two (fitting) terms influence the evolution of the curve.

4.4.3 Extension of Level Set Formulation to Vector Valued Images

The proposed Chan-Vese model assumes homogeneous regions for accurate segmentation. As mentioned earlier, the regions of acute stroke are characterized by intensity inhomogeneity and shape complexity. Therefore, in order to better segment the stroke regions, the above model was applied in our problem with a key difference. The pixel value, instead of being a scalar u_0, is a vector with the b2000 and ADC values being the vector elements. Such a formulation helps incorporate the information from both the b2000 and the ADC map, both of which discriminate the infarct pixels from the normal ones in the data. A bright pixel on the b2000 scan along with a reduced value on the ADC map is significant indicator of an infarct pixel. Accordingly, the standard Chan-Vese formulation is modified as

$$\begin{aligned}
&\hat{F}(c1, c2, c3, c4, C) = \mu \cdot Length(C) + \nu \cdot Area(\omega) \\
&+ \lambda_1 \int_{\omega} |u_d(x, y) - c_1|^2 dxdy + \lambda_2 \int_{\Omega \setminus \bar{\omega}} |u_d(x, y) - c_2|^2 dxdy \\
&+ \lambda_3 \int_{\omega} |u_a(x, y) - c_3|^2 dxdy + \lambda_4 \int_{\Omega \setminus \bar{\omega}} |u_a(x, y) - c_4|^2 dxdy
\end{aligned} \tag{4.2}$$

where, $\mu, \nu, \lambda_1, \lambda_2, \omega, \Omega, C$ are as defined before, $\lambda_3, \lambda_4 > 0$ are tuning parameters, $u_d : \bar{\Omega} \rightarrow \mathbb{R}$ is the b2000 DWI image and $u_a : \bar{\Omega} \rightarrow \mathbb{R}$ is the corresponding ADC map. The constants ($c1$, $c3$) and ($c2$, $c4$) dependent on C are the averages of (u_d, u_a) inside C and outside C respectively. We fix $\lambda_1 = \lambda_2 = \lambda_3 = \lambda_4 = 1$ and $\nu = 0$ and the segmentation is the minimization of the energy functional $\hat{F}(c1, c2, c3, c4, C)$.

Since the active contour based approach can lead to erroneous boundaries for small-sized lesions ($< 1\%$ of image size), an ADC-based post-processing of the small-sized segmented results is done as described in Section 4.3.3.

4.5 Experiments & Analysis of Segmentation Results

4.5.1 Materials Used

As described earlier in section 3.4.1, DWI volumes of confirmed stroke patients were collected from two local hospitals which had different types of scanners and used different methods of data acquisition. In addition to the 24 volumes used for analysis of the auto-windowing method, 17 more volumes were collected amounting to a total of 41 volumes for analysis of segmentation results. The detailed data description can be seen in Table 4.1.

Table 4.1: Data Description of the DWI Volumes Collected from the Two Local Hospitals With Different Types of Scanners and Different Acquisition Protocols.

Scanner	Data-sets	Acquired Data	Voxel Size	Matrix Size/Pixel Depth (PD)
Scanner-1	29	b=0, b=1000, b=2000, ADC = Post Acquisition (Sequential)	0.98×0.98 ×6.32mm	256×256×22 /PD=16 bits
Scanner-2	12	b=0, b=1000, b=2000, ADC = During Acquisition (Simultaneous)	1.95×1.95 ×7.28mm	128×128×20 /PD=12 bits

4.5.2 Experiments & Analysis of Results

4.5.2.1 Quantitative Validation of Segmentation Results

In order to evaluate the proposed framework for segmentation, true-positives (TP), false-positives (FP), false-negatives (FN) and true-negatives (TN) were determined. Sample colour coded segmented results are shown in Figure 4.3. The colour code is as follows: blue, red and green pixels indicate TP, FP and FN pixels, respectively. Blue pixels dominate the results, indicating the robustness of the algorithm in accurately capturing different-sized lesions in the data.

The Dice coefficient (DC) [43] measures the spatial overlap between the GT and the results of segmentation. A value of zero indicates no overlap, while a value of one represents a perfect overlap. The sensitivity (SN) and specificity (SP) figures were also calculated. The statistics of DC, SN and SP are

Table 4.2: Descriptive Statistics & Evaluation Metrics to Quantitatively Validate the Segmentation Results.

Statistics	Sensitivity (%)	Specificity (%)	DC
Maximum	97.30	99.99	0.96
Minimum	43.75	99.01	0.41
Mean	83.68	99.79	0.81
Median	87.07	99.90	0.84
Std	10.58	0.25	0.12
CV	0.1264	0.0025	0.1530

$DC = 2 * \frac{A \cap G}{A \cup G}$	$SN = \frac{TP}{TP+FN}$	$SP = \frac{TN}{FP+TN}$

presented in Table 4.2. In DC calculation, A is the segmented volume by the algorithm and G is the ground truth. The coefficient of variation (CV) reported here is the ratio of the standard deviation (Std) and the mean values. Ideal value of CV is 0 and DC is 1. These are reported to observe the trend in the results.

Our dataset contained 324 large-sized lesions and 286 small-sized lesions. In light of this fact, the high median values of SN, SP and DC with corresponding low CV values indicate that the segmentation algorithm is robust to size and shape variations in lesions. The datasets were acquired from two different scanners with different acquisition protocols and the algorithm appears to be robust to these factors.

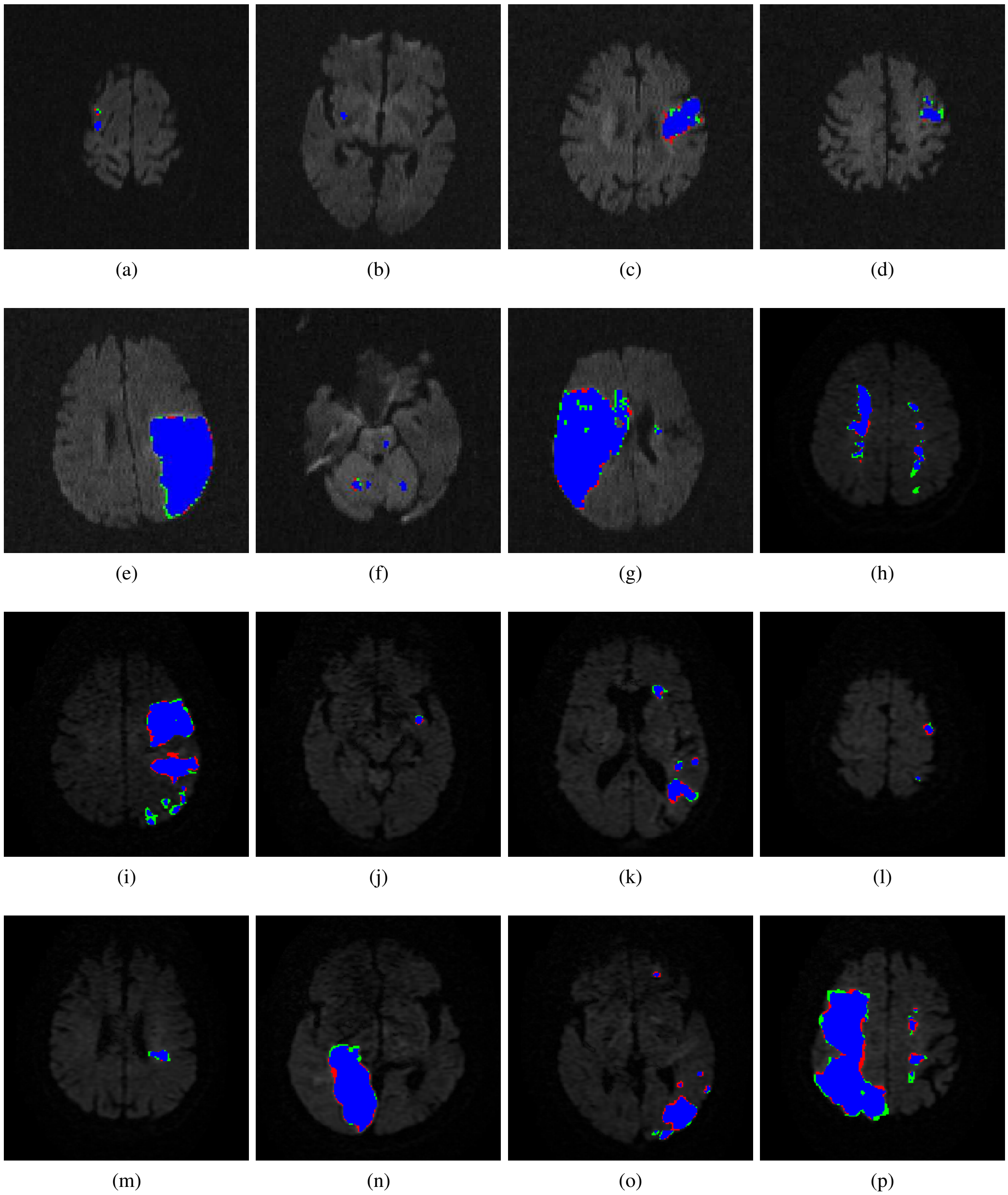

Figure 4.3: Colour Coded Segmentation Results shown overlaid on b2000 data, Blue:TP, Red:FP and Green:FN.

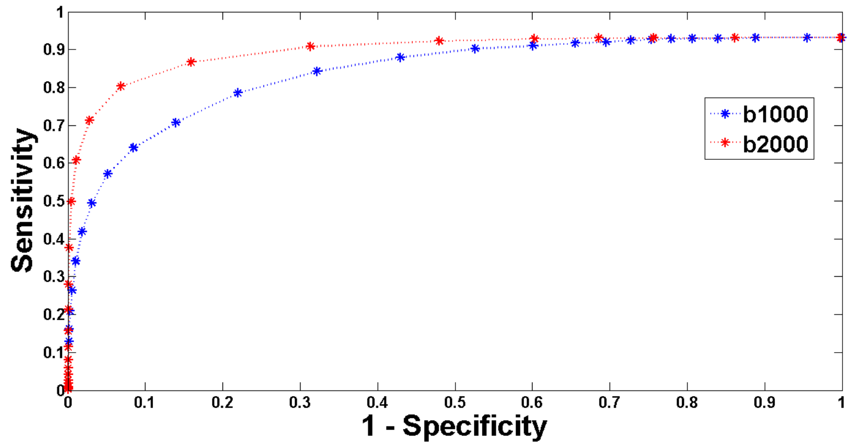

Figure 4.4: Detection performance of the proposed framework for small-sized stroke lesions.

4.5.3 Performance Evaluation of Proposed Framework

Receiver Operator Characteristics (ROC) gives a measure of the diagnostic accuracy of a proposed framework. A point on the ROC plot gives the sensitivity achieved by the method against the given specificity for a given parameter setting. Thus, varying the control parameter used in the approach generates the ROC plot which describes the trend in the obtained sensitivity and specificity values for the approach. The ROC is generated by plotting the $sensitivity$ against the $(1 - specificity)$. The $sensitivity$ is a measure of how correctly the method identifies the true candidates while $(1 - specificity)$ is a measure of how many false candidates the method identifies. Ideally, the $sensitivity$ should be high for a low value of $(1 - specificity)$.

4.5.3.1 Utility of b2000 in Detection

The first experiment aimed at determining the effectiveness of b2000 data in lesion *detection*. Sample results of detection on b1000, b2000 and the proposed method (using b1000, b2000 and the ADC data) are shown in Figure 4.6. As seen from the figure, the detection results on b1000 data fail to capture all the lesions, specially the small-sized lesions in areas of white matter tracts which is primarily due to the poor contrast between the lesion and the normal brain tissue. Detection improves on b2000 data but low SNR results in large number of false positives mostly in areas of white matter tracts with reduced diffusion which appear hyperintense. The proposed method accurately captures all the lesion locations as b1000 and the ADC information help reject the false positives.

For a quantitative assessment of performance, receiver operating characteristic (ROC) curves were generated for detection of small lesions ($< 1\%$ image size) by varying the knee-point described in Section 3.3.2. The obtained plots are shown in Figure 4.4 for detection with only b1000 or b2000. The plot shows that b2000 is more effective for detecting small, early ischemic changes. This is consistent with the qualitative results and with findings reported in [23].

4.5.3.2 Utility of b2000 in Segmentation

First the segmentation performance on b1000 was compared with that on b2000. The segmented results were assessed for only true lesion locations (found from GT), across the volumes. The median Dice coefficients (DC) were found to be 0.68 (b1000) and 0.83 (b2000). Thus, b2000 appears to be effective for segmentation as well, providing an improvement of 22.06% in DC value.

4.5.3.3 Assessment of Segmentation With Different Variants of the Proposed Framework

The performance evaluation aimed at a differential analysis with respect to size of the lesions, comparing the ROC plots between 4 methods - (i) Method described in [8] (ii) Segmentation on lesion candidates obtained on b1000 (iii) Segmentation on lesion candidates obtained on b2000 (iv) Segmentation on lesion candidates obtained utilizing b1000, b2000 & ADC (our method). Based on the lesion size, for all the methods, the ROC plots were generated for the following cases - (a) segmentation of small-sized ($<$1% of image size) lesions (b) segmentation of large-sized ($>$1% of image size) lesions (c) segmentation of all the lesions in the data. For method (i), the intensity threshold for finding the segmented candidates was varied to generate the ROC plot. For methods (ii), (iii), (iv), the threshold for finding the candidate lesions was varied to generate the ROC plots. Once the candidate lesions were obtained, the segmentation was performed using the level set approach. The obtained plots for ROC for the methods are shown in Figure 4.5. Area under the ROC curve (AUC) is a measure of the accuracy of the method. A method is said to be *excellent* if the AUC $>$ 0.90. Table 4.3 shows the AUC for the four methods for all the cases. Along with the AUC, the 95% confidence interval (CI) for the ROC is specified for each case. Since a high specificity is expected to achieve high accuracy in stroke segmentation, the sensitivity values at 95% specificity are also reported in Table 4.3 to study the trend among the methods for the different cases. As expected in a typical ROC plot, a steep rise in the curve is seen for all the plots which indicates that high sensitivity is achieved for a small number of false positives. This validates the accuracy of all the methods in segmenting the stroke lesions for all the cases.

For segmentation results of all the lesions, a comparison in the ROC plots of the methods shows that methods (i) & (ii) utilizing only b1000 data perform poorly relative to the methods (iii) & (iv). A significant improvement is observed in the performance of methods (iii) & (iv) utilizing b2000 data over methods (i) & (ii) which confirms the effectiveness of processing on b2000 data over b1000 data. Method (iv) utilizing the b1000 & ADC data along with the b2000 data shows the best performance among the four methods, which shows slight improvement over method (iii) utilizing only b2000 data. This confirms the effectiveness of the b1000 data and ADC in the pipeline. The sensitivity and specificity values of stroke lesion segmentation are dominated due to high accuracy in segmentation of large sized lesions in the data. Low accuracy in the segmentation of small sized lesions does not significantly affect the overall sensitivity and specificity values. In this regard, all the four methods perform *excellently*, as seen from Table 4.3. The trend in the results of segmentation for small versus large lesions in the data is seen the ROC plots as shown in Figure 4.5. For the segmentation results of large lesions, the trend

Table 4.3: Performance of Different Methods based on the Lesion Size in terms of Area Under the Curve (AUC), 95% Confidence Interval (CI) and Sensitivity at 95% Specificity. (i), (ii), (iii), (iv) correspond to method in [8], framework on b1000, b2000 and both b1000 & b2000 respectively.

	Small-Sized Lesions			
	(i)	(ii)	(iii)	(iv)
AUC	0.923	0.873	0.932	**0.955**
95% CI	0.914-0.931	0.862-0.883	0.923-0.941	**0.947-0.962**
Sensitivity	0.715	0.651	0.752	**0.841**

	Large-Sized Lesions			
	(i)	(ii)	(iii)	(iv)
AUC	0.974	0.964	0.982	**0.986**
95% CI	0.972-0.975	0.963-0.966	0.980-0.983	**0.985-0.987**
Sensitivity	0.902	0.903	0.945	**0.955**

	All Lesions			
	(i)	(ii)	(iii)	(iv)
AUC	0.967	0.957	0.977	**0.987**
95% CI	0.965-0.968	0.955-0.958	0.975-0.978	**0.986-0.988**
Sensitivity	0.865	0.891	0.942	**0.961**

is similar as to that for the case of all the lesions. Methods (iii) & (iv) outperform methods (i) & (ii), again signifying the use of b2000 over b1000 data. Method (iv) gives the highest values of the AUC. For segmentation of small lesions in the data, as seen from the ROC plots in Figure 4.5, a significant distinction in the performance of the proposed method over the other methods is observed. Method (ii) performs worst and an improvement over it is shown by method (i). Method (ii) fails at the detection stage in accurately identifying the small stroke lesions on b1000 data. A large number of false-positives at the detection stage affect the results of segmentation. Further false-positives add to the number at the segmentation stage since the conspicuity of the small lesions on b1000 data is poor. Method (i), on the other hand, performs segmentation as the final step and hence less false-positives and improved results are observed as compared to method (ii). Both the methods (i) & (ii) operating on b1000 data underperform relative to method (iii) operating on b2000 data. However, only slight improvement is shown by method (iii) over these methods. A significant improvement in the results is shown by method (iv). This highlights the strength of our method in accurately segmenting the smallest regions of infarction in the data.

As seen from Figure Table 4.3 and 4.5, the values of AUC and CI for all the cases are highest for method (iv). Although the improvement in the value of AUC for the proposed approach may not be significant relative to other methods for segmenting all the stroke lesions in the data, the proposed method is able to capture small sized lesions accurately which are missed by the other methods. This is

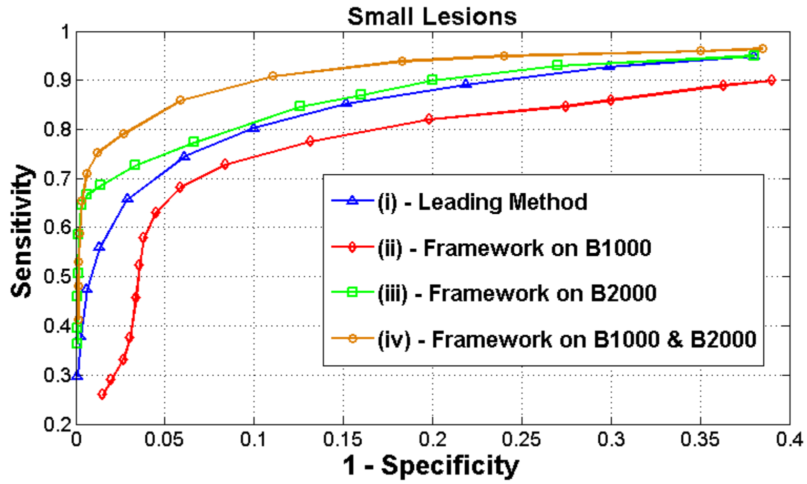

(a)

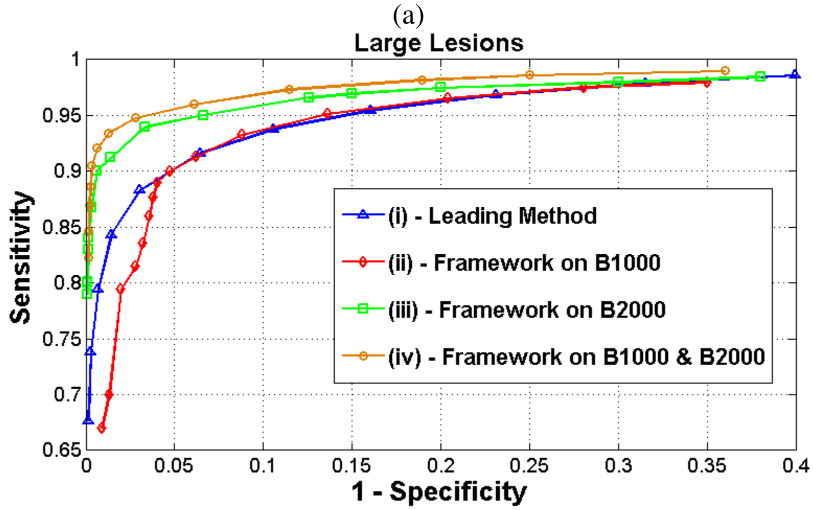

(b)

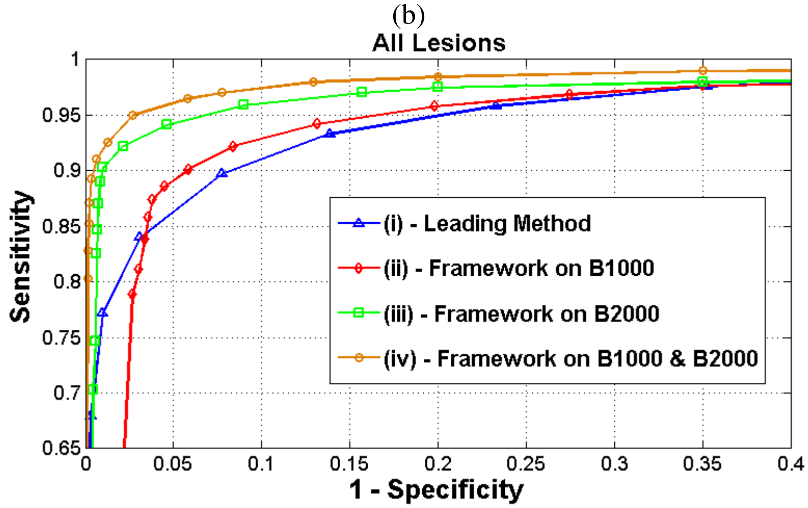

(c)

Figure 4.5: Segmentation performance of the proposed framework. ROC plots for (a) small lesions (<1% image size), (b) large lesions (>1% image size) and (c) all lesions present in the data.

a crucial aspect from a diagnostic point of view where the primary objective is to capture all the lesions regardless of their size and location.

The trend in the ROC curve is affected by results of both the detection and the segmentation stage. As seen from Figure 4.4, utilization of b2000 data outperforms that on b1000 data at the detection stage. As described in *Experiment 2*, utilizing b2000 data significantly improves the segmentation accuracy as compared against b1000 data at the segmentation stage. Hence a significant difference in the performance of methods (i), (ii) (which utilize b1000 data) and methods (iii), (iv) (which utilize b2000 data) is seen. Utilizing the b1000 data and the ADC in method (iv) is shown to improve the performance even further among all the cases. Previous experiments were performed to validate the effectiveness of utilizing b2000 data at the detection and segmentation stage independently. However, the ROC analysis validates, the effectiveness of the complete pipeline, utilizing the ADC & b1000 data along with the b2000 data which achieves the best performance among the four methods. From this analysis, it can be concluded that utilization of b2000 data offers significant improvement both at the detection and the segmentation stage while utilizing it in the proposed framework along with the b1000 data and the ADC achieves the best results.

4.5.4 Qualitative Analysis of Detection and Segmentation Results

A comparison in the qualitative results of detection on b1000, b2000 and the integrated framework utilizing, b1000, b2000 and the ADC data respectively, is shown in Figure 4.6. As seen from the figure, the detection results on b1000 data fail to capture all the lesions, specially the small-sized lesions in areas of white matter tracts. This is primarily due to the poor contrast between the lesion and the normal brain tissue provided by the b1000 data. b2000 data provides improved lesion contrast over b1000 data at the cost of low SNR and hence the high detectability is accompanied with large number of false positives. These false positives occur mostly in areas of white matter tracts with reduced diffusion that appear hyperintense on the b2000 data. These false positives at the detection stage, later, affect the segmentation accuracy of the results. The integrated framework utilizing the b1000, b2000 and the ADC data accurately captures all the lesion locations. The false positives captured on the b2000 data are addressed in the candidate refinement stage by exploiting the b1000 and the ADC data.

The knee-point detection method described in Section 3.3.2 roughly captures the threshold for detection of candidate lesions on the b1000 data. Since the b1000 data provides poor contrast between the lesion and the normal brain tissue, the estimated threshold fails to capture small-sized lesions with subtle intensity changes. b2000 data, on the other hand, provides improved lesion contrast which enables the knee-point detection method to almost accurately threshold the candidate lesions. Qualitative results shown in Figure 4.6 and quantitative results shown in Figure 4.4 validate this hypothesis. Thus, it can be concluded that the b2000 data significantly improves the detection results over b1000 data while the integrated framework utilizing b1000, b2000 and the ADC data is useful in addressing the false positives and providing with accurate stroke lesion detection results.

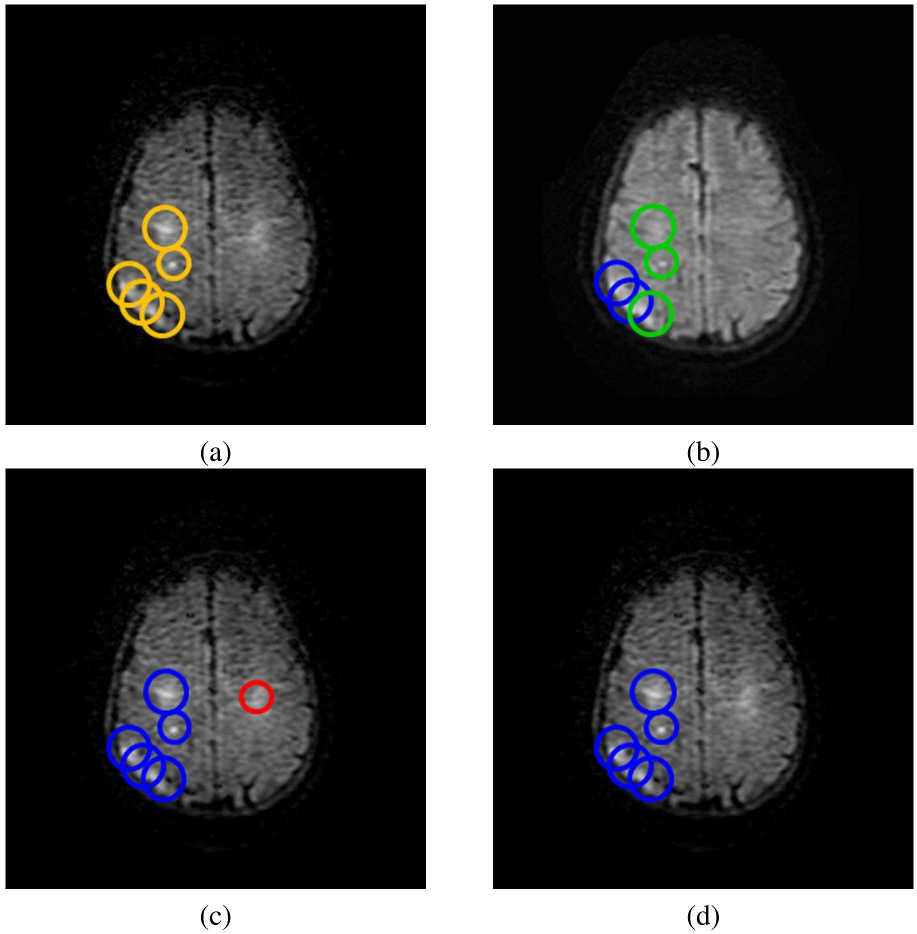

Figure 4.6: (a) Ground truth for stroke lesion locations. Detection results on (b) b1000 data (c) b2000 data and (d) integrated framework. Blue:TP, Red:FP and Green:FN.

The detection stage identifies the core of the lesion and the segmentation stage improves on the lesion definition at the boundaries. Thus, the accuracy of the segmented results is directly dependent on the accuracy of the detection results. Figure 4.7 shows a comparison in the qualitative segmentation results of (i) Method described in [8] (ii) Segmentation on lesion candidates obtained on b1000 (iii) Segmentation on lesion candidates obtained on b2000 (iv) Segmentation on lesion candidates obtained utilizing b1000, b2000 & ADC (our method). Method (i) completely fails to capture the small-sized lesions and the significantly-sized lesion is captured with poor accuracy. A similar result is observed for the result of method (ii) operating on b1000 data alone. The Chan-Vese model of active contour depends on the mean intensity difference between the inside and the outside of the evolving contour. Due to poor lesion contrast on b1000 data, the contour evolution in the Chan-Vese framework is affected which results in poor lesion definition of the segmented results. Dominant green pixels in the Figure 4.7(a) & (b) suggests poor sensitivity of the segmentation results. Significantly improved results are observed on the b2000 data with high sensitivity as compared to those on b1000 data, however at the cost of false positives for method (iii). Since false positives are observed in the detection stage on b2000

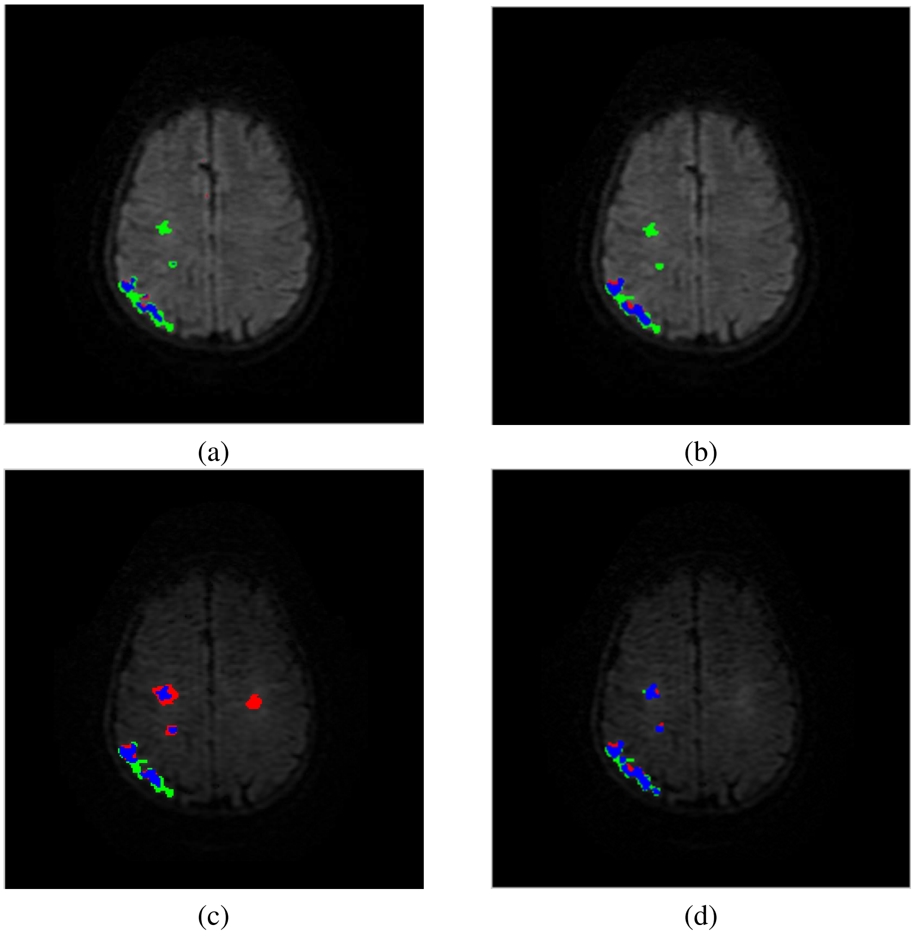

Figure 4.7: Colour Coded Segmentation Results results on (a) [8] method, proposed framework for (b) b1000, (c) b2000 and (d) integrated approach respectively. Blue:TP, Red:FP and Green:FN.

data, the segmentation results are also affected as seen from the dominant red pixels in Figure 4.7(c). Method (iv) achieves the best segmentation results as seen from the dominant blue pixels in Figure 4.7(d). Method (iv) improves upon the accurately detected lesion cores to obtain accurate segmentation results. The auto-windowing helps improve the lesion contrast which aids in the contour evolution to achieve accurate lesion definition of the segmented results. In conclusion, the segmentation accuracy is largely dependent on the detection accuracy. The contour evolution in the Chan-Vese framework improves with better lesion contrast. Thus, operating on b2000 data during segmentation is beneficial as compared to that on the b1000 data. The auto-windowing helps improve the lesion contrast significantly, thus improving the lesion definition and aiding the contour evolution for accurate segmentation results.

4.6 Discussion & Conclusions

A novel technique for segmentation of stroke lesions in brain DWI data using multiple b-values (b1000 & b2000) and the ADC maps is presented. The method is robust to data acquired on multiple scanners with different acquisition processes. The qualitative and quantitative results reported in the study show superiority of the method in accurately detecting and segmenting the stroke lesions over the conventional methods operating only on the b1000 data. The median DC, sensitivity and specificity for stroke segmentation were 0.84, 87.07% and 99.90% respectively. The method is automated and therefore could assist the clinicians in diagnosis.

The improvement in performance of the proposed method comes at the expense of computational cost due to the need to process additional data. However, in stroke cases where there are only small-sized lesions, the gain to be obtained in correctly detecting (and segmenting) the presence of the lesion can outweigh the additional computational burden.

Chapter 5

Conclusions

A novel technique for segmentation of stroke lesions in brain DWI data using multiple b-values (b1000 & b2000) and the ADC maps is presented in this thesis. This is in contrast to earlier approaches where the processing is done on single b-valued DWI data. A method which integrates the information from multiple b-values for better characterization of the stroke lesions is attempted in the study.

The presented solution for stroke detection and segmentation is proposed in three major stages -

- Lesion Detection
- Data Pre-processing
- Lesion Segmentation

Lesion Detection: The novelty in utilizing the information from multiple b-valued data to characterize stroke lesions and address the false positives is presented in chapter 4. This is achieved by exploiting the improved lesion sensitivity and contrast of the high b-valued data, the low anisotropy effects on the low b-valued data and the impermeability of the ADC to shine-through artifacts. This method is able to capture the lesion locations in the data accurately.

Data Pre-processing: Chapter 3 describes the concept and implementation of this stage which employs a novel, automated windowing technique that significantly improves the contrast of ischemic stroke lesions present in the DWI scan. The novelty in the approach is the enhancement of the data relative to the ischemic lesions in the data. Since the proposed method of windowing is general, the scope of the method can be extended to enhancement of the data relative to any set of candidates present in the data, especially in medical data where multiple types of lesions might be present.

Lesion Segmentation: Chapter 4 introduces the *Lesion Segmentation* stage which utilizes the modified Chan-Vese approach to segment the stroke lesions in the data. The modification made to the Chan-Vese approach is to adapt to the information fusion from the DWI and the ADC data which improves the segmentation results. The obtained results show that the modified approach is able to accurately segment the stroke regions regardless of their size and outperforms the traditional methods which operate on single b-valued data.

The strength of the proposed method is it's ability to capture the smallest regions of infarction in the data which are often missed by the conventional methods. This aids the clinicians in diagnosis and helps them to study the lesion patterns and predict the stroke evolution and likely outcome. The method is robust to data acquired on multiple scanners with different acquisition processes. The qualitative and quantitative results reported in the study show superiority of the method in accurately detecting and segmenting the stroke lesions over the conventional methods operating only on the b1000 data. The median DC, sensitivity and specificity for stroke segmentation were 0.84, 87.07% and 99.90% respectively.

The improvement in performance of the proposed method comes at the expense of computational cost due to the need to process additional data through multiple stages. The implementation was done in MATLAB [28] run on a 64-bit machine on a 2.2 GHz processor. It took 40-90 seconds to process a given volume data. The processing time is directly proportional to the number of slices affected by the stroke in the data since segmentation was performed only on these slices. Since the method performs segmentation at a slice level, the processing time can be drastically reduced by utilizing a parallel implementation on a GPU framework using the CUDA architecture. However, in stroke cases where there are only small-sized lesions, the gain to be obtained in correctly detecting (and segmenting) the presence of the lesion can outweigh the additional computational burden.

Accurate evaluation of presence of infarct and its extent is most important in the setting of acute stroke in the window period for thrombolytic therapy (< 3 hours after onset). After eliminating the risk of intra-cerebral haemorrhage the acute stroke is diagnosed for the region of DWI-PWI (diffusion-perfusion) mismatch to classify the tissue at risk. The perfusion weighted imaging (PWI) represents a quantitative data and hence the region of interest (penumbra of the stroke region) can be obtained easily. On the other hand, extracting the region of interest on the DWI (core of the stroke region) requires manual delineation of the boundary of the stroke region by expert radiologists. Such a task depends on the availability of experienced radiologists in emergency setting of acute stroke and is time consuming. Hence, an automated framework which can accurately detect and segment the stroke lesions will aid the radiologist in a faster and accurate diagnosis.

Imaging with higher b-value does not incur any additional costs and only adds 20-40 seconds to the scan time on a standard 1.5 Tesla scanner. Few of the hospitals follow it as a standard protocol to acquire DWI acquisition with b1000 and b2000 data. This helps the radiologist to confirm the presence of ischemic stroke on b1000 data in case of doubt. Thus, the proposed framework can be easily utilized in the clinical setting of acute stroke since it'll automate the process of stroke segmentation on DWI data. The overhead of the additional time incurred for imaging with multiple b-values and the time taken for the method to generate results is significantly less than the time taken for manual delineation of the stroke regions by the experienced radiologist. The proposed method, therefore, could assist the clinicians in diagnosis of acute stroke.

Related Publications

Conference Publications

1. Mujumdar S, Sivaswamy J, Varma R, Kishore LT. **Auto-windowing of Ischemic Stroke Lesions in Diffusion Weighted Imaging of the Brain.** *Indian Conference on Medical Informatics and Telemedicine, ICMIT, March 28-30, 2013, IIT, Kharagpur, India.* **Oral Presentation**.
2. Mujumdar S, Sivaswamy J, Varma R and Kishore LT. **A Novel Framework for Segmentation of Stroke Lesions in Diffusion Weighted MRI Using Multiple b-Value Data.** *International Conference on Pattern Recognition, ICPR, Nov 11-15, 2012, Tsukuba, Japan.* **Oral Presentation**.
3. Kaushik S, Mujumdar S and Sivaswamy J. **Adaptive Intensity Windowing for MR Images.** *Proceedings of The Workshop in conjunction with Indian Conference on Computer Vision, Graphics and Image Processing (ICVGIP'10), 12-15 Dec. 2010, IIT, Delhi, India.* **Poster Presentation**.

Journals in Preparation

1. Mujumdar S, Sivaswamy J, Varma R and Kishore LT. **Detection and Segmentation of Stroke Lesions from Multiple b-Value Diffusion Weighted MRI Data.**
2. Mujumdar S, Sivaswamy J, Varma R and Kishore LT. **A Novel Technique for Auto-windowing of DW-MRI to Assist Clinicians in Stroke Diagnosis.**

Bibliography

[1] The internet stroke center.

[2] Stroke association of victoria.

[3] H. Bagher-Ebadian et al. Predicting final extent of ischemic infarction using artificial neural network analysis of multi-parametric mri in patients with stroke. *PloS one*, 6(8):e22626, 2011.

[4] A. Baird and S. Warach. Magnetic resonance imaging of acute stroke. *Journal of Cerebral Blood Flow & Metabolism*, 18(6):583–609, 1998.

[5] P. Barber et al. Identification of major ischemic change: diffusion-weighted imaging versus computed tomography. *Stroke*, 30(10):2059–2065, 1999.

[6] I. Belykh and C. Cornelius. Method for automated window-level settings for magnetic resonance images, May 15 2007. US Patent 7,218,763.

[7] K. Bhanu Prakash et al. Identification, segmentation, and image property study of acute infarcts in diffusion-weighted images by using a probabilistic neural network and adaptive gaussian mixture model. *Academic radiology*, 13(12):1474–1484, 2006.

[8] K. Bhanu Prakash et al. Automatic processing of diffusion-weighted ischemic stroke images based on divergence measures. *CARS*, 3(6):559–570, 2008.

[9] T. Chan and L. Vese. Active contours without edges. *TIP*, 10(2):266–277, 2001.

[10] M. Delano and Y. Cao. High b-value diffusion imaging. *Neuroimaging Clinics of North America*, 12(1):21, 2002.

[11] J. Eastwood et al. Quantitative assessment of the time course of infarct signal intensity on diffusion-weighted images. *American journal of neuroradiology*, 24(4):680–687, 2003.

[12] J. Fiebach et al. Ct and diffusion-weighted mr imaging in randomized order. *Stroke*, 33(9):2206–2210, 2002.

[13] M. Fisher. Antithrombotic and thrombolytic therapy for ischemic stroke. *Journal of thrombosis and thrombolysis*, 7(2):165–169, 1999.

[14] P. Grammaticos, A. Diamantis, et al. Useful known and unknown views of the father of modern medicine, hippocrates and his teacher democritus. *Hell J Nucl Med*, 11(1):2–4, 2008.

[15] P. Hagmann, L. Jonasson, P. Maeder, J. Thiran, V. Wedeen, and R. Meuli. Understanding diffusion mr imaging techniques: From scalar diffusion-weighted imaging to diffusion tensor imaging and beyond1. *Radiographics*, 26(suppl 1):S205–S223, 2006.

[16] Y. Han, E. Li, J. Tian, J. Chen, H. Wang, and J. Dai. The application of diffusion-and perfusion-weighted magnetic resonance imaging in the diagnosis and therapy of acute cerebral infarction. *International Journal of Biomedical Imaging*, 2006:1–11, 2006.

[17] J. Hopyan, A. Ciarallo, D. Dowlatshahi, P. Howard, V. John, R. Yeung, L. Zhang, J. Kim, G. MacFarlane, T. Lee, et al. Certainty of stroke diagnosis: Incremental benefit with ct perfusion over noncontrast ct and ct angiography1. *Radiology*, 255(1):142–153, 2010.

[18] M. Jacobs et al. Unsupervised segmentation of clinical stroke with multiparameter mri. *Proc. Intl. Soc. Mag. Reson. Med*, 8:669, 2000.

[19] M. Jacobs, T. Ibrahim, and R. Ouwerkerk. Mr imaging: Brief overview and emerging applications. *Radiographics*, 27(4):1213–1229, 2007.

[20] B. G. Jarvis. Direct-rt. *MediaLab (Version 2012) [Computer Software]*, 2012.

[21] Y. Kabir et al. Multimodal mri segmentation of ischemic stroke lesions. *Engineering in Medicine and Biology Society, 2007. EMBS 2007. 29th Annual International Conference of the IEEE*, pages 1595–1598, 2007.

[22] A. Khademi, A. Venetsanopoulos, and A. Moody. Automatic contrast enhancement of white matter lesions in flair mri. *Biomedical Imaging: From Nano to Macro, IEEE International Symposium on*, pages 322–325, 2009.

[23] H. Kim et al. High-b-value diffusion-weighted mr imaging of hyperacute ischemic stroke at 1.5 t. *AJNR*, 26(2):208–215, 2005.

[24] D. Le Bihan et al. Artifacts and pitfalls in diffusion mri. *Journal of magnetic resonance imaging*, 24(3):478–488, 2006.

[25] W. Li et al. Robust unsupervised segmentation of infarct lesion from diffusion tensor mr images using multiscale statistical classification and partial volume voxel reclassification. *Neuroimage*, 23(4):1507–1518, 2004.

[26] P. Lyden, M. Lu, C. Jackson, J. Marler, R. Kothari, T. Brott, and J. Zivin. Underlying structure of the national institutes of health stroke scale: results of a factor analysis. *Stroke*, 30(11):2347–2354, 1999.

[27] A. Martel et al. Measurement of infarct volume in stroke patients using adaptive segmentation of diffusion weighted mr images. *Medical Image Computing and Computer-Assisted Intervention–MICCAI99*, pages 22–31, 1999.

[28] MATLAB. *version 7.11.0.584 (R2010b)*. The MathWorks Inc., Natick, Massachusetts, 2010.

[29] A. McKinney, M. Teksam, R. Felice, S. Casey, R. Cranford, C. Truwit, and S. Kieffer. Diffusion-weighted imaging in the setting of diffuse cortical laminar necrosis and hypoxic-ischemic encephalopathy. *American journal of neuroradiology*, 25(10):1659–1665, 2004.

[30] S. Mehta, S. Chaudhury, A. Bhattacharyya, and A. Jena. A soft-segmentation visualization scheme for magnetic resonance images. *Magnetic resonance imaging*, 23(7):817–828, 2005.

[31] J. Meyer, A. Gutierrez, B. Mock, D. Hebron, J. Prager, M. Gorey, and D. Homer. High-b-value diffusion-weighted mr imaging of suspected brain infarction. *American journal of neuroradiology*, 21(10):1821–1829, 2000.

[32] N. Montiel et al. Robust nonparametric segmentation of infarct lesion from diffusion-weighted mr images. *EMBS*, pages 2102–2105, 2007.

[33] D. Mumford and J. Shah. Optimal approximations by piecewise smooth functions and associated variational problems. *Communications on pure and applied mathematics*, 42(5):577–685, 1989.

[34] D. Na, V. Thijs, G. Albers, M. Moseley, and M. Marks. Diffusion-weighted mr imaging in acute ischemia: value of apparent diffusion coefficient and signal intensity thresholds in predicting tissue at risk and final infarct size. *American journal of neuroradiology*, 25(8):1331–1336, 2004.

[35] R. Pereira et al. Effect of b value on contrast during diffusion-weighted magnetic resonance imaging assessment of acute ischemic stroke. *JMRI*, 15(5):591–596, 2002.

[36] N. Saad et al. Automated segmentation of brain lesion based on diffusion-weighted mri using a split and merge approach. *Biomedical Engineering and Sciences (IECBES), 2010 IEEE EMBS Conference on*, pages 475–480, 2010.

[37] M. Sasaki, M. Ida, K. Yamada, Y. Watanabe, and M. Matsui. Standardizing display conditions of diffusion-weighted images using concurrent b0 images: a multi-vendor multi-institutional study. *Magnetic Resonance in Medical Sciences*, 6(3):133–137, 2007.

[38] R. Sener. Diffusion mri: apparent diffusion coefficient (adc) values in the normal brain and a classification of brain disorders based on adc values. *CMIG*, 25(4):299–326, 2001.

[39] S. Shen, A. Szameitat, and A. Sterr. Detection of infarct lesions from single mri modality using inconsistency between voxel intensity and spatial locationa 3-d automatic approach. *Information Technology in Biomedicine, IEEE Transactions on*, 12(4):532–540, 2008.

[40] B. Stein et al. Statistical and deformable model approaches to the segmentation of mr imagery and volume estimation of stroke lesions. *MICCAI*, pages 829–836, 2001.

[41] M. Vidaurrazaga, L. Diago, and A. Cruz. Contrast enhancement with wavelet transform in radiological images. *Engineering in Medicine and Biology Society. Proceedings of the 22nd Annual International Conference of the IEEE*, 3:1760–1763, 2000.

[42] H. Yang, Y. Lee, Y. Fan, and H. Taso. A novel algorithm of local contrast enhancement for medical image. *Nuclear Science Symposium Conference Record. NSS'07. IEEE*, 5:3951–3954, 2007.

[43] K. Zou et al. Statistical validation of image segmentation quality based on a spatial overlap index. *Academic Radiology*, 11(2):178–189, 2004.